https://doi.org/10.5194/egusphere-2023-2877
Preprint. Discussion started: 8 December 2023

Northern vs. southern hemisphere differences in the stratospheric influence on variability in tropospheric nitrous oxide

Cynthia D. Nevison[1], Qing Liang[2], Paul A. Newman[2], Britton B. Stephens[3], Geoff Dutton[4,5], Xin Lan[4,5], Roisin Commane[6], Yenny Gonzalez[7,8], Eric Kort[9]

[1]Institute for Arctic and Alpine Research, University of Colorado, Boulder, CO, USA
[2]NASA Goddard Space Flight Center, Greenbelt, MD, USA
[3]NSF National Center for Atmospheric Research, Boulder, CO, USA
[4]Global Monitoring Laboratory, NOAA Earth System Research Laboratory, Boulder, CO, USA
[5]Cooperative Institute for Research in Environmental Sciences (CIRES), University of Colorado, Boulder, CO, USA
[6]Department of Earth & Environmental Sciences, Lamont-Doherty Earth Observatory, Columbia University, Palisades, NY, USA
[7]CIMEL Electronique, Paris, 75011, France
[8]Izana Atmospheric Research Center, AEMET, Santa Cruz de Tenerife, 38001, Spain
[9]Department of Climate & Space Sciences & Engineering, University of Michigan, Ann Arbor, MI, USA

Correspondence to: Cynthia D. Nevison (cynthia.nevison@colorado.edu)

Abstract. We present a chemistry-climate model with a tagged stratospheric nitrous oxide (N_2O) tracer that predicts distinct seasonal cycles in tropospheric N_2O caused by descent of N_2O-depleted stratospheric air in polar regions. We identify similar phenomena in recently available aircraft profiles from global campaigns and routine monitoring. Long-term atmospheric measurements from the National Oceanic Atmospheric Administration (NOAA) global surface monitoring network provide additional support for a significant impact on surface N_2O originating from the stratosphere. In the northern hemisphere, the NOAA surface N_2O atmospheric growth rate anomaly is negatively correlated with the previous winter's polar lower stratospheric temperature. This negative correlation is consistent with increased (decreased) transport in years with a strong (weak) Brewer Dobson circulation of warm, N_2O-depleted air from the middle and upper stratosphere into the lower stratosphere, with subsequent cross-tropopause transport of the N_2O-depleted air into the troposphere. In the southern hemisphere, polar lower stratospheric temperature is correlated to monthly summertime anomalies in tropospheric N_2O as it descends into its seasonal minimum, a result that is supported by aircraft data as well as the chemistry-climate model. However, the N_2O atmospheric growth rate anomaly in the southern hemisphere is better correlated to the stratospheric quasi-biennial oscillation (QBO) index, as well as the El Niño Southern Oscillation index, than to polar lower stratospheric temperature. These hemispheric differences in the factors influencing the N_2O atmospheric growth rate are consistent with known atmospheric dynamics and the complex interaction of the QBO with the Brewer Dobson circulation.

https://doi.org/10.5194/egusphere-2023-2877
Preprint. Discussion started: 8 December 2023

1 Introduction

Nitrous oxide (N_2O) is an important ozone-depleting substance and long-lived greenhouse gas, with a global warming potential (GWP) of 265 relative to CO_2 over a 100 year time horizon (*WMO*, 2018). N_2O has an atmospheric lifetime of about 120 years and is destroyed slowly in the stratosphere by both photolysis and oxidation, with a fraction of the oxidation product yielding NO_x, a catalyst of stratospheric ozone destruction (*Crutzen,* 1970; *Prather et al.,* 2015). N_2O has abundant natural microbial sources in soil, freshwater and oceans, which account for the majority of global emissions, although anthropogenic sources are becoming increasingly important (*Canadell et al*., 2021).

The atmospheric N_2O concentration has risen from about ~270 ppb preindustrially to 336 ppb by 2022 (*MacFarling-Meure et al*., 2006; *Lan et al.,* 2022). This rise has been attributed largely to the Haber-Bosch process of industrial N fixation for the production of agricultural fertilizer, which has increased the N substrate available to nitrogen cycling microbes (*Park et al.*, 2012). Recent evidence suggests that N_2O is increasing at an accelerating rate in the atmosphere, possibly due to a nonlinear response of microbes to increasing N inputs in intensively fertilized agricultural systems (*Thompson et al.*, 2019; *Liang et al.*, 2022).

Interannual variability in the atmospheric growth rate (AGR) and small-amplitude seasonal cycles (in the range of 0.1 – 0.3% of the background mixing ratio) are detectible in the high precision N_2O measurements made in recent decades (*Nevison et al*., 2004; 2007; 2011; *Jiang et al*., 2007; *Thompson et al.*, 2013). A few studies have inferred information about surface biogeochemical sources based on the observed seasonal cycle in atmospheric N_2O. However, these studies have cautioned that the transport of N_2O-depleted air from the stratosphere is a major cause of both seasonal and interannual variability in surface N_2O, which complicates the interpretation of surface emission signals (*Nevison et al.*, 2005; 2011; 2012; *Thompson et al.*, 2014; *Ray et al.*, 2020; *Ruiz et al.*, 2021). Other studies have argued that El Niño Southern Oscillation (ENSO) cycles are likely the major driver of interannual variability in tropospheric N_2O (*Ishijima et al.*, 2009; *Thompson et al*., 2013) or that ENSO-driven variability can obscure the influence of the stratosphere in some years (*Ruiz et al.*, 2021).

Studies of the stratospheric influence on surface N_2O variability have differed with respect to the relative impact on the Northern Hemisphere (NH) vs. Southern Hemisphere (SH). *Ray et al.* (2020) found direct correlations between the stratospheric QBO at 50 hPa, lagged 8-12 months, and the observed NOAA surface station N_2O AGR, but in the SH only. They hypothesized that the correlation of QBO and N_2O AGR was less evident in the NH due to the increased influence of surface emissions. *Ruiz et al.* (2021) found that, despite a clear QBO correlation to N_2O loss rates in the tropical middle stratosphere, variability in N_2O at the surface appeared to be governed by stratosphere-troposphere exchange (STE) dynamics in the lowermost stratosphere, rather than directly by the QBO. They showed evidence for a coherent influence of STE on the surface N_2O seasonal cycle in the NH but not the SH. *Nevison et al.* (2011) argued for a STE-driven N_2O seasonal minimum

https://doi.org/10.5194/egusphere-2023-2877
Preprint. Discussion started: 8 December 2023

in both hemispheres, based on significant correlations between surface N_2O seasonal anomalies and stratospheric temperature as well as polar vortex breakup indices.

A better grasp of the controls on tropospheric N_2O variability has potentially important implications for the interpretation of biogeochemical signals in N_2O data. If abiotic factors associated with the downward transport of N_2O-depleted air from the stratosphere contribute significantly to variability, they must be disentangled from the data before inferring information about surface biogeochemistry and emissions. Understanding the influence of stratospheric variability on surface N_2O also may provide insight into anomalous changes in the AGR of CFC-11, which has a stratospheric sink similar to that of N_2O (*Ray et al.*, 2020; *Ruiz et al.*, 2021; *Lickley et al.*, 2021).

This paper analyzes the causes of interannual variability in both the seasonal cycle and the AGR of tropospheric N_2O. The methodology includes examination of vertical profiles of atmospheric N_2O, collected by aircraft campaigns and routine monitoring, and analysis of output from the Goddard Earth Observing System Chemistry-Climate Model (GEOSCCM). This model couples the GEOS general circulation model (GCM) to a full atmospheric chemistry module (Nielsen et al., 2017) and has been modified to distinguish a stratospheric N_2O tracer from tropospheric tracers of fresh surface emissions (*Liang et al.*, 2022). GEOSCCM is shown to indicate a profound and dominant influence of the stratosphere on the tropospheric N_2O seasonal cycle, with similar patterns to those observed in aircraft data. A correlation analysis is performed on the surface N_2O AGR observed by NOAA and two indices of stratospheric variability as well as the El Niño Southern Oscillation (ENSO) index. A similar correlation analysis is performed with output from GEOSCCM, which simulates its own QBO. The correlation analyses support the importance of the stratospheric influence on interannual variability in surface N_2O but also suggest a role for ENSO-driven variability in the SH.

2 Methods

2.1 GEOSCCM with tagged stratospheric tracers

The GEOS-5 chemistry climate model (GEOSCCM) was used to simulate atmospheric N_2O with geographically resolved surface emissions from soil, ocean and anthropogenic sources, and full stratospheric chemistry with stratospheric N_2O destruction due to photolysis and $O(^1D)$ oxidation (*Nielsen et al.,* 2017). The model was run at 1°x1° resolution with 72 vertical layers from the surface to 0.01 hPa. In addition to the standard chemistry mechanism, four N_2O tracers were included to track: 1) aged air from the stratosphere ($N2O_{ST}$), and 2) soil, 3) ocean, and 4) anthropogenic sources freshly emitted in the troposphere following the same approach as in *Liang et al.* (2008) for chlorofluorocarbons (CFCs). $N2O_{ST}$ was used to provide a model estimate of the stratospheric influence on tropospheric N_2O mean seasonal cycles, while a total N_2O tracer was defined to include the influences of both stratospheric destruction and surface sources. The full GEOSCCM simulation spanned 2000-2019 (*Liang et al.*, 2022). The climatological seasonal cycle was analyzed based on the last 5 years of the simulation. The full 20-year simulation was used in the correlation analysis between model surface N_2O anomalies and QBO and polar lower

https://doi.org/10.5194/egusphere-2023-2877
Preprint. Discussion started: 8 December 2023

stratospheric temperature (PLST). GEOSCCM temperature and QBO are both internally generated by the GEOS GCM and do not necessarily correspond to observations. However, they were computed in the same way as the observed indices, as described below in Section 2.4.1 and 2.4.2, respectively.

2.2 N_2O Data

2.2.1 Surface N_2O from NOAA long-term monitoring sites

Surface atmospheric N_2O data from the late 1990s onward were obtained from the NOAA Global Monitoring Laboratory (GML) for comparison to GEOSCCM output. NOAA has two programs that measure N_2O, the Halocarbons and other Atmospheric Trace Species (NOAA/HATS) (*Thompson et al.*, 2004) and the Carbon Cycle Greenhouse Gases group (NOAA/CCGG). NOAA/HATS provides *in situ* data measured every ~ 60 minutes using the Chromatograph for Atmospheric Trace Species (CATS) instruments at 5 baseline sites. NOAA/CCGG maintains a flask-air sampling network at ~55 widely distributed surface sampling sites, in which duplicate samples are collected about weekly and shipped to Boulder, Colorado for analysis by gas chromatography (GC) with electron capture detection and by a Tunable Infrared Laser Direct Absorption Spectroscopy (TILDAS) after August, 2019. The instruments are calibrated with a suite of standards on the WMO X2006A scale maintained by NOAA GML (*Hall et al.*, 2007). Uncertainties of the measurements (68% confidence interval) range from 0.26 to 0.43 ppb with GC-ECD and 0.16 ppb with TILDAS. The mean uncertainties in the CATS GC data are 0.2 to 1.2 ppb (68% confidence interval) over most of the 2000s, with an increase in recent years as the instruments near their lifetime.

This study used the NOAA combined HATS/CCGG N_2O product from 1998-2020 (https://doi.org/10.15138/GMZ7-2Q16), which is based on monthly medians from the CATS *in situ* program (at 5 sites) and monthly means from the CCGG flask program (at 13 background sites). The combined monthly data are first aggregated at the measurement program level for each sampling location. If both HATS and CCGG measure at a location, a weighted mean is calculated based on the programs' monthly uncertainties. In addition to the individual sites, global and hemispheric means are estimated from the latitude-binned and mass-weighted means of the combined monthly means for 12 background sites (*Hall et al.*, 2011).

2.2.2 NOAA Empirical Background for atmospheric N_2O

The NOAA empirical background (EBG) is a 4-dimensional (4-D) field, constructed from NOAA surface and aircraft N_2O data, which is used in North American regional inversions to represent the background concentration of atmospheric N_2O prior to the influence of continental surface fluxes (*Nevison et al.*, 2018). The EBG is defined daily over North America from 500-7500 m every 1000 m, from 170°-50°W every 10° longitude and from 20-70°N every 5° latitude (or, prior to 2017, from 20-80°N every 10° latitude). To construct the 4-D field, NOAA data are categorized as marine boundary layer, free troposphere

https://doi.org/10.5194/egusphere-2023-2877
Preprint. Discussion started: 8 December 2023

or continental boundary layer, depending on the location of each sample. These three categories are treated individually as follows: For the marine boundary layer, time- and latitude-dependent reference surfaces are computed separately for the Pacific and Atlantic (*Masarie and Tans*, 1995, updated as described in *Lan et al.*, 2023). For the free-troposphere, reference surfaces are created using a similar approach, with an additional "domain-filling" step informed by backward and forward trajectories for each aircraft sample collected above 3000 magl. For the continental boundary layer, N_2O data are detrended by subtracting the latitude and time dependent marine boundary layer reference values, where the transition from Pacific to Atlantic is represented by linear interpolation as a function of longitude across the continent. Then, a multi-year mean seasonal cycle is computed as a function of latitude, longitude and day of year using local Kriging following (*Hammerling et al.,* 2012).

2.2.3 QCLS atmospheric N_2O data from vertical profiling campaigns

Atmospheric N_2O measurements have been made *in situ* with the Harvard/Aerodyne Quantum Cascade Laser Spectrometer (QCLS) on a variety of aircraft campaigns designed to study the atmospheric profiles of greenhouse and related gases (*Wofsy et al.*, 2011; *Stephens et al.*, 2018). QCLS N_2O data are retrieved at 1-Hz with 1s precision of 0.09 ppb and reproducibility with respect to the WMO N_2O scale of 0.2 ppb (*Kort et al., 2011; Santoni et al., 2014*) on the NOAA-2006 scale (*Hall et al.*, 2007). The first of the vertical profiling campaigns used here, the HIAPER Pole to Pole Observations (HIPPO) project, consisted of 5 roughly month-long sets of flights centered over the central Pacific Ocean extending from the surface to the upper troposphere/lower stratosphere and nearly pole to pole. These flights were timed between January 2009 and November 2011 to create a climatological seasonal cycle (*Wofsy et al.*, 2011). The second campaign (ORCAS), took place in January-February 2016 and focused specifically on the Southern Ocean south of ~35°S (*Stephens et al*., 2018). Most recently, the Atmospheric Tomography Mission (ATom) campaign extended nearly pole to pole over both the Pacific and Atlantic Oceans. ATom consisted of four ~month-long sets of flights over 3 years, timed to create a climatological seasonal cycle (*Thompson et al.*, 2022). QCLS N_2O was measured during ATom deployments 2-4 in January/February 2017, September/October, 2017 and April/May 2018, respectively (*Gonzalez et al.*, 2021). (Note: technical issues interfered with the N_2O measurements on the ATom-1 deployment in July/August 2016).

2.3 Correlation analysis for surface N_2O

2.3.1 Interannual variability in the atmospheric growth rate

Interannual variability in the atmospheric growth rate of surface N_2O at NOAA surface monitoring sites was calculated by first removing the seasonal cycle from the monthly mean time series by computing a 12-month running average,

$$X_i = (C_{i-6} + 2\sum_{k=i-5}^{i+5} C_k + C_{i+6})/24, \quad (1)$$

https://doi.org/10.5194/egusphere-2023-2877
Preprint. Discussion started: 8 December 2023

where C is the original monthly mean time series and X is the deseasonalized time series. The slope of the deseasonalized time series then was computed as a central difference,

$$S_i = 12\ \frac{x_{i+1}-x_{i-1}}{2}, \quad (2)$$

where S is the centrally differenced slope and the scalar 12 converts S from units of ppb/month to ppb/yr. To account for the increasing growth rate of atmospheric N_2O observed over the 21st Century (*Liang et al.*, 2022), the absolute slopes S were converted to atmospheric growth rate anomalies by removing an optimal (increasing) linear fit determined by recursive least squares regression. The atmospheric growth rate (AGR) anomalies constituted a monthly-resolved time series, which was plotted against various proxies and indices for both stratospheric influences and ENSO, as described below. Least squares linear regression correlation coefficients and p-values were computed with the assumption that a p-value < 0.05 was statistically significant at the 95% confidence level.

2.3.2 Interannual variability in the magnitude of the seasonal N_2O minimum

To calculate interannual anomalies in the magnitude of the seasonal minimum, the raw monthly mean N_2O data were detrended with a 3rd-order polynomial and a climatological seasonal cycle was constructed by taking the average of the detrended data for all Januaries, Februaries, etc. This climatological annual cycle was subtracted from the original raw data to produce a deseasonalized (but not detrended) time series. A running 12-month annual mean of this curve was then computed as in Equation 1, but where C is now the deseasonalized time series rather than the original monthly mean time series. At stations with gaps in the monthly data, the original 3rd order polynomial fit was used as a placeholder in the running mean. The running mean was subtracted from the deseasonalized curve to remove the secular trend and other low frequency variability, thus isolating the residual high frequency anomalies.

The high frequency residuals were sorted by month and selected months were plotted against the PLST BDC proxy described in Section 2.4.1. The months selected were those surrounding the seasonal N_2O minimum, which is the most distinct feature of the seasonal cycle at remote baseline NOAA sites and which were hypothesized, based on previous work, as most likely to be influenced by the descent of N_2O-depleted air from the stratosphere (*Nevison et al.*, 2011). (Note: strong local sources can create large seasonal signals in atmospheric N_2O that dominate the stratospheric influence at some sites, e.g., those influenced by agriculture or coastal upwelling (*Lueker et al.*, 2003; *Nevison et al.*, 2018; *Ganesan et al.*, 2020)).

The monthly N_2O anomaly analysis was applied only to PLST BDC proxy and not to the QBO or ENSO indices, because the latter are monthly indices for which it is not straightforward to choose a representative month to correlate to the N_2O anomaly,

https://doi.org/10.5194/egusphere-2023-2877
Preprint. Discussion started: 8 December 2023

given that the anomaly might result from the cumulative effect over multiple months. PLST in contrast has one unique value each year that can be plotted against that year's N_2O anomaly for any given month.

2.4 Proxies and indices for the correlation analysis

2.4.1 Polar lower stratospheric temperature as proxy for the Brewer Dobson circulation

Mean polar (60°-90°) lower stratospheric temperature at 100 hPa in winter/spring (January-March in the NH and spring (September-November) in the SH was computed from MERRA-2 reanalyses (*Gelaro et al.,* 2017). PLST reflects the cumulative effect of fall/winter stratospheric downwelling. The mean PLST in each hemisphere was treated as a proxy for the integrated strength of the BDC, which brings warm N_2O-depleted air from the middle to upper tropical stratosphere into the polar winter lower stratosphere, with warmer PLST corresponding to stronger downwelling (*Nevison et al.*, 2007; 2011). Winter months were averaged in the NH and spring months in the SH to account for the later seasonal breakup of the Antarctic polar vortex compared to the Arctic polar vortex (*Nevison et al.*, 2011). For the monthly analysis, the PLST proxy was regressed against the monthly N_2O anomaly in each of the subsequent months leading up to and encompassing the seasonal minimum in atmospheric N_2O, which occurs in summer in the NH and autumn in the SH. For the AGR analysis, the mean N_2O AGR anomaly was averaged over 12 months (considering a range of start/end months) for regression against PLST.

2.4.2 Quasi-Biennial Oscillation (QBO)

The QBO is a tropical, lower stratospheric, downward-propagating zonal wind variation with an average period of ~28 months that dominates the variability of tropical lower stratospheric meteorology (*Baldwin et al*., 2001; *Butchart*, 2014). The QBO was quantified using monthly mean stratospheric zonal wind values in m/s derived from twice daily balloon radiosondes conducted by the Meteorological Service Singapore Upper Air Observatory at a station located at 1.34°N, 103.89°E (https://acd-ext.gsfc.nasa.gov/Data_services/met/qbo/QBO_Singapore_Uvals_GSFC.txt). A positive QBO indicates westerly winds and a negative QBO indicates easterly winds. A range of altitudes from 10 mb to 100 mb was considered. Since the QBO index is a monthly mean time series, it can be compared directly to the monthly mean N_2O AGR time series. However, delays are expected between the QBO and its influence on tropospheric N_2O (*Strahan et al.*, 2015; *Ray et al.*, 2020). Therefore, a range of lag times was considered spanning 6-24 months when correlating with the N_2O AGR anomalies to identify the optimal QBO altitude and lag in each hemisphere.

2.4.3 ENSO

The El Niño Southern Oscillation (ENSO) index refers to the oscillation between warm (El Niño) and cold (La Niña) phases in the eastern tropical Pacific Ocean. El Niño is a periodic warming and deepening of the thermocline in the eastern tropical Pacific associated with westerly wind anomalies that excite eastward propagating downwelling equatorial Kelvin waves

https://doi.org/10.5194/egusphere-2023-2877
Preprint. Discussion started: 8 December 2023

(*McPhadden et al.*, 1998). The Niño 3.4 index, which is based on sea surface temperature anomalies from 5°S to 5°N and 170° to 120°W, defines an El Niño event as a temperature anomaly of > 0.4 degrees C. Conversely, the index defines a temperature anomaly of < -0.4°C defines as a La Niña event. Monthly Niño 3.4 indices were obtained from https://www.cpc.ncep.noaa.gov/data/indices/sstoi.indices. Like the QBO index, Niño 3.4 is a monthly time series that can be compared directly to the monthly mean N_2O AGR time series. In the comparison presented here, a range of lag times in the Niño 3.4 index was considered spanning 0-12 months to identify the optimal lag in each hemisphere.

2.5 GEOSCCM correlation analysis

Equations 1 and 2 were applied to GEOSCCM N_2O output sampled at the coordinates of NOAA monitoring sites to create modeled N_2O AGR time series and monthly anomalies, using both total N_2O and N_2O_{ST}. Similarly, mean winter and spring PLST at 100 hPa was calculated for GEOSCCSM output in the NH and SH, as described in Section 2.4.1, for each model year from 2000-2019. Finally, a GEOSCCM monthly QBO index was calculated at a range of altitudes from 10 mb to 100 mb by averaging the model zonal wind component in m/s between 5°S and 5°N over each of the 240 months from 2000-2019. A correlation analysis was performed using the GEOSCCM N_2O AGR and monthly anomaly time series regressed against GEOSCCM PLST and QBO, similar to that described for the observed quantities in Sections 2.3-2.4. (Note: the ENSO correlation analysis was not applied to GEOSCCM output because the model did not attempt to reproduce the impact of ENSO on surface flux variability (*Liang et al.*, 2022).)

3. Results

3.1 Stratospheric influence on tropospheric N_2O in model and aircraft data

GEOSCCM simulates a strong stratospheric influence on the surface N_2O seasonal cycle in both hemispheres, in which air depleted in N_2O accumulates during winter in the polar lower stratosphere and crosses the tropopause in springtime (early summer) in the NH (SH) (Figure 1). The N_2O depleted air moves downward and mixes equatorward from January to May at SH mid-to-high latitudes and from March to August at NH mid-to-high latitudes. Due to these lags in downward propagation and mixing, the surface minimum in the lower troposphere is not felt until autumn in both hemispheres (Figure 2).

https://doi.org/10.5194/egusphere-2023-2877
Preprint. Discussion started: 8 December 2023

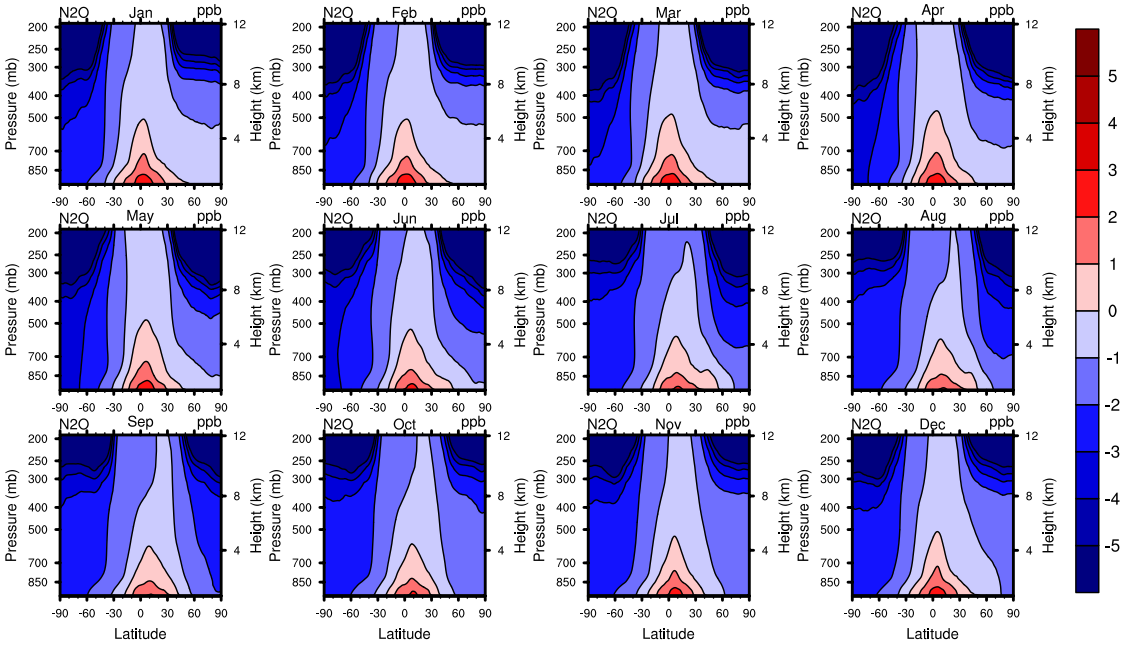

Figure 1: GEOSCCM N_2O anomalies plotted in a monthly sequence of latitude vs. altitude plots extending from the surface up to 30 hPa (about 24 km). The GEOSCCM N_2O fields are detrended based on a deseasonalized fit to the model time series sampled at Mauna Loa and the mean value at Mauna Loa is removed to create the anomalies.

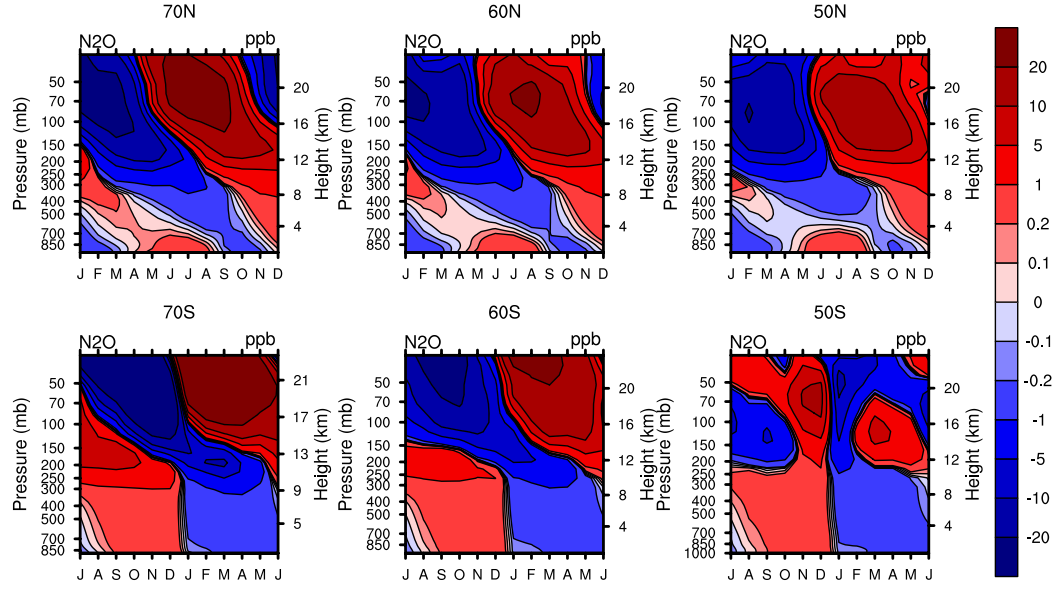

Figure 2: GEOSCCM N_2O anomalies vs. month over a mean seasonal cycle, plotted from the surface to 30 hPa in the northern (top row) and southern (bottom row) hemispheres. The GEOSCCM N_2O fields are detrended based on the model time series sampled at the latitude, longitude and altitude of Mauna Loa. Zonal averages are computed at 70°, 60° and 50° latitude bins in each

https://doi.org/10.5194/egusphere-2023-2877
Preprint. Discussion started: 8 December 2023

hemisphere and pressure level. Monthly anomalies are then computed by subtracting the annual mean value at each pressure level. The SH panels are plotted with a 6 month shift to facilitate comparison of the seasonal phasing relative to the NH.

The GEOSCCM seasonal cycle in tropospheric N_2O is dominated by stratospheric loss that is transported to the surface, rather than by the influence of emissions from soil, ocean and anthropogenic sources, although the surface emissions tend to pull the total N_2O seasonal minimum about 1 month earlier than the $N2O_{ST}$ minimum (Figure 3). Comparison to data at long-term monitoring sites suggests that GEOSCCM captures the mean seasonal cycle in N_2O relatively well in the Southern Hemisphere but overestimates the amplitude of the cycle at high northern latitudes, with a ~1-2 month delay in phasing relative to observations (Figure 3).

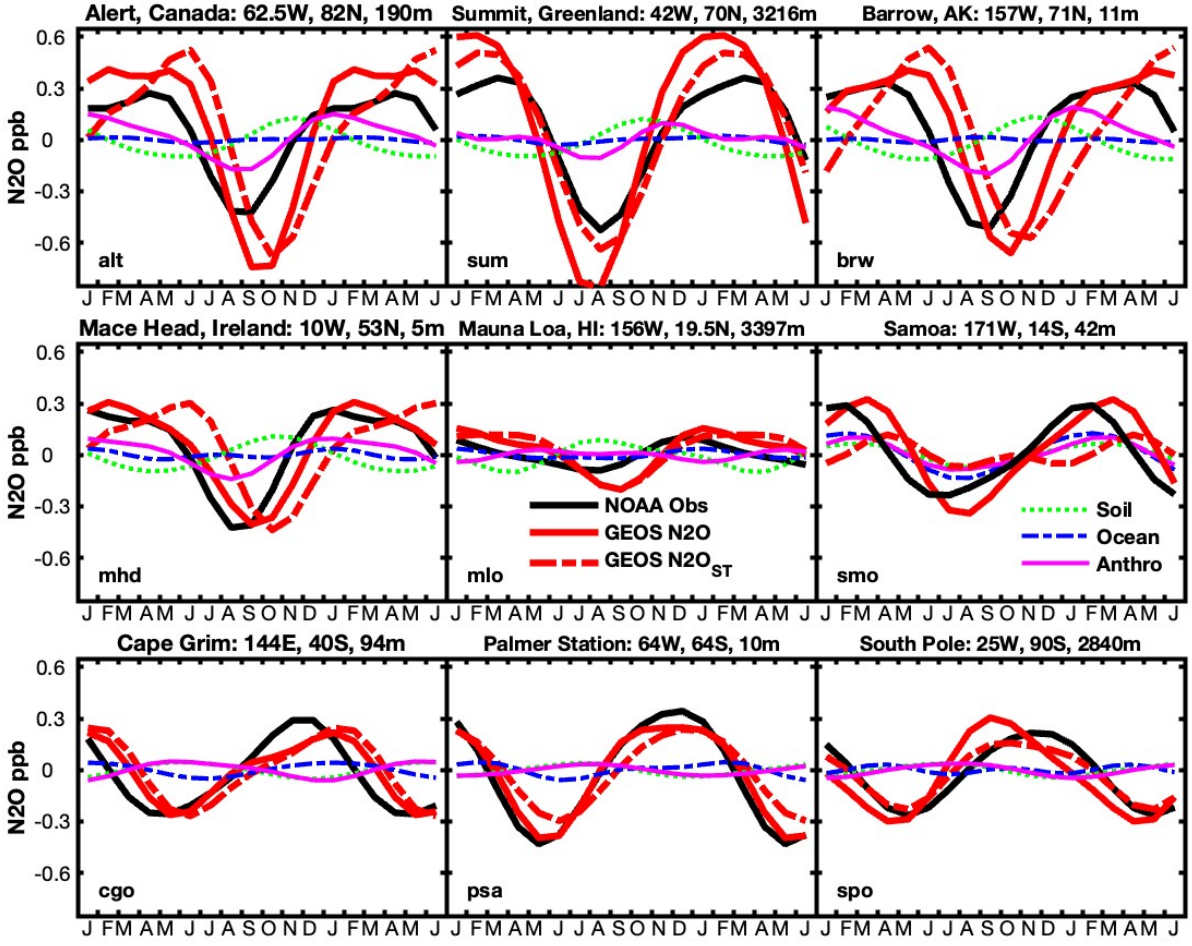

Figure 3: Detrended seasonal cycles in atmospheric N_2O modeled by GEOSCCM and compared to NOAA surface station data at 9 surface sites. The red line is total N_2O from all forcings, while the dashed red line is the tagged stratospheric tracer N_2O_{ST}. The black heavy line is observed N_2O. Surface anomalies are shown for natural soil (green), ocean (blue), and anthropogenic, including agriculture, industry and biomass burning (magenta) surface emission sources.

https://doi.org/10.5194/egusphere-2023-2877
Preprint. Discussion started: 8 December 2023

The NOAA N_2O empirical background has similar features to those simulated by GEOSCCM. When viewed as a 12-month sequence of NH altitude vs. latitude contours, extending up to 8 km, the NOAA data indicate that the North American background signal of stratospheric depletion originates at polar latitudes in the upper troposphere in spring and is felt in the midlatitude lower troposphere by July, with a peak influence around August (Figure 4). The effect on the troposphere is strongest near the pole and weakens substantially moving equatorward. A comparison of altitude vs. month contours for GEOSCCM and NOAA suggests a faster, more direct propagation of the stratospheric signal down to the surface in the NOAA data compared to the model (Figure 5). As a result, the phasing of the GEOSCCM surface minimum is delayed ~1-2 months relative to the NOAA empirical background, consistent with the comparison to NOAA surface monitoring data in Figure 3.

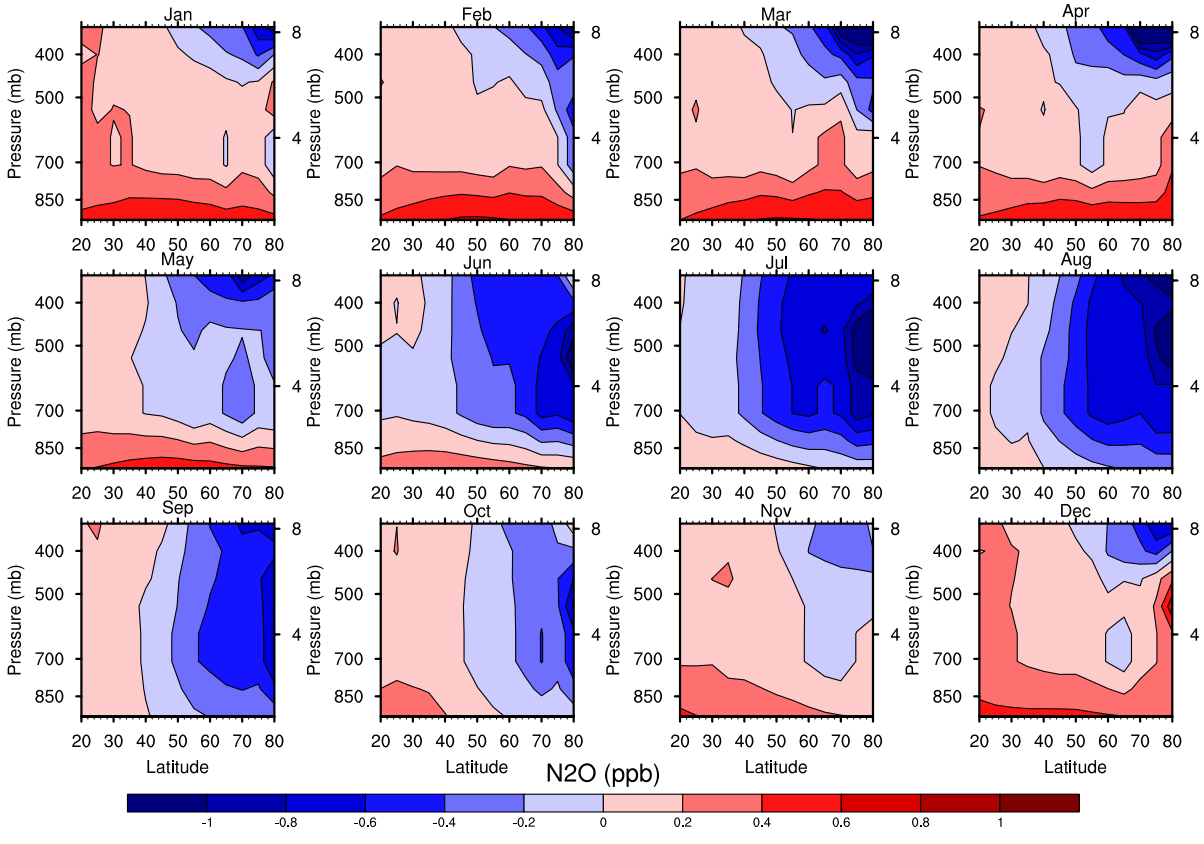

Figure 4: Northern hemisphere N_2O anomalies from the NOAA empirical background based on NOAA regularly sampled aircraft flights, plotted in a monthly sequence of altitude vs. latitude plots extending up to ~8 km (330 hPa) and from 20° to 80°N, zonally averaged over 160 to 60°W. The NOAA N_2O fields are detrended based on a deseasonalized fit to the observed time series sampled at the latitude, longitude and altitude of Mauna Loa.

https://doi.org/10.5194/egusphere-2023-2877
Preprint. Discussion started: 8 December 2023

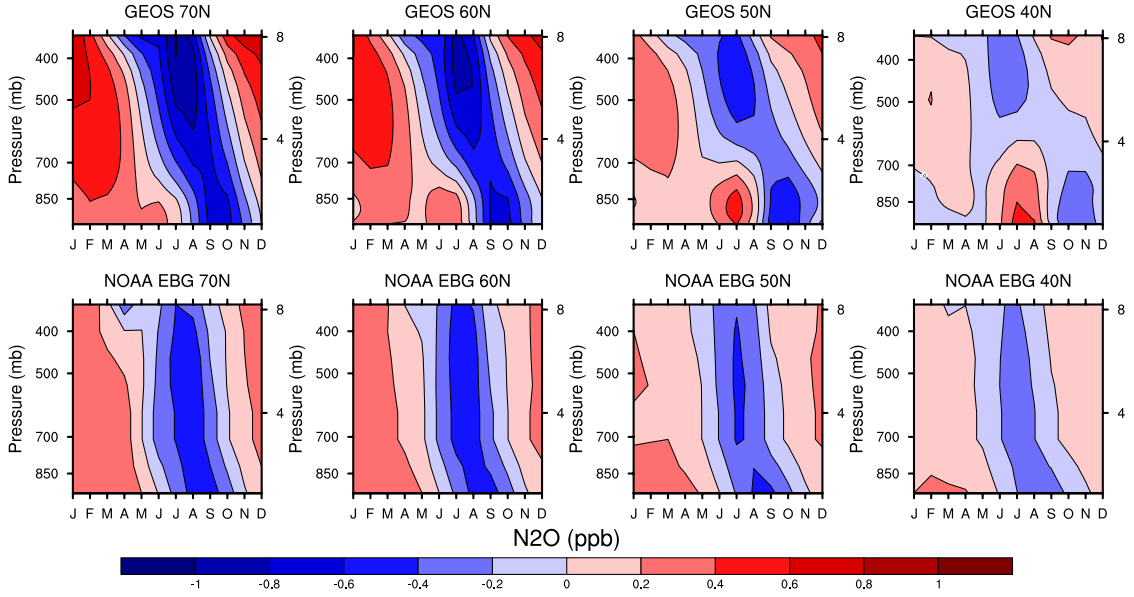

Figure 5: Northern hemisphere N_2O anomalies vs. month over a mean seasonal cycle, plotted over the height of the troposphere up to ~8 km (330 hPa), comparing GEOSCCM (top row) and the NOAA empirical background (bottom row) at 70°, 60°, 50° and 40°N zonally averaged 10° latitude bins. The GEOSCCM and NOAA N_2O fields are detrended based on their respective time series sampled at Mauna Loa for model and observations, respectively. Monthly anomalies are computed by subtracting the annual mean value at each pressure level.

HIPPO aircraft data extend up to 14 km and thus provide a broader perspective with respect to altitude of the stratospheric influence on tropospheric N_2O, but with sparser temporal coverage than the NOAA empirical background. The southbound transects from the five HIPPO deployments, when detrended and arranged chronologically over an annual mean cycle, form a sequence that is most readily seen in the NH (Figure 6). N_2O-depleted air accumulates in the polar lower stratosphere in January and crosses the tropopause by March/April. By June it has descended into the troposphere and moved equatorward, reaching its maximum influence at the surface in August. By October/November, the stratospheric signal is no longer visible at the surface following tropospheric mixing and dilution. Notably, this seasonal progression is less apparent although still discernible in a fuller dataset that also includes the ATom and northbound HIPPO transects (Supplementary Figure 1).

https://doi.org/10.5194/egusphere-2023-2877
Preprint. Discussion started: 8 December 2023

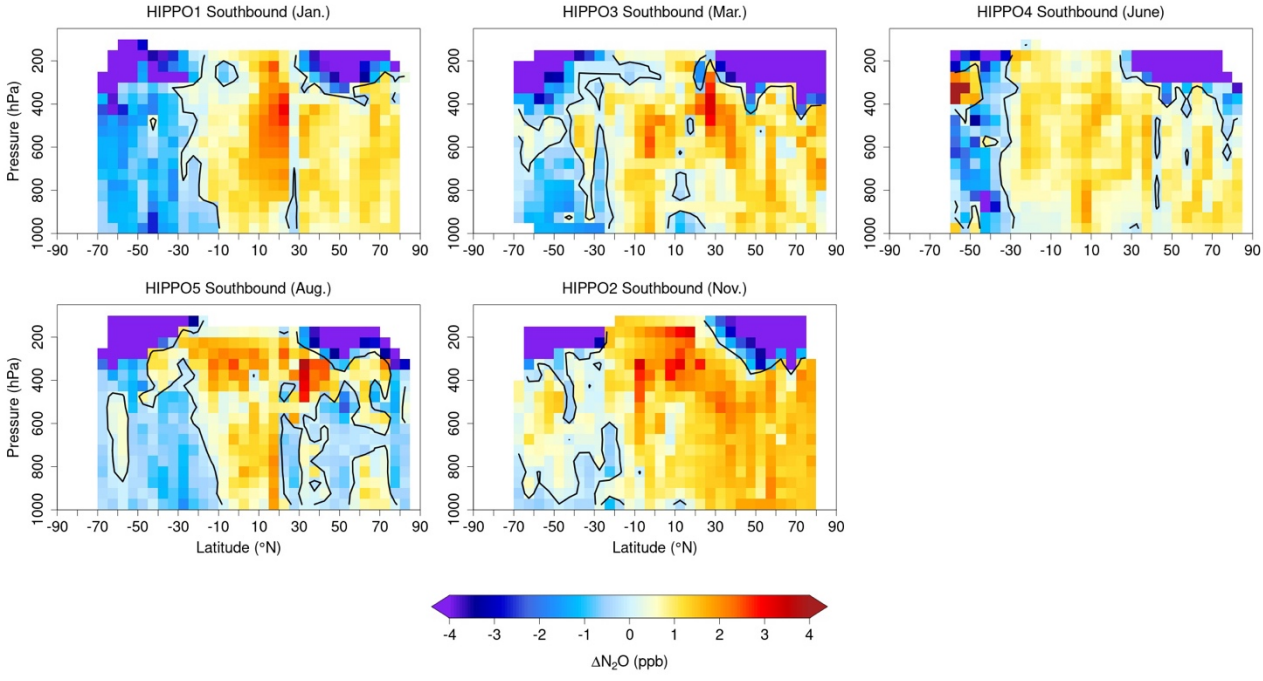

Figure 6: Sequence of five southbound HIPPO transects arranged to form an annual sequence. Flight track data were interpolated onto a 5 degree latitude by 50 hPa grid using the akima package in R (Akima, 1978). A deseasonalized fit to the NOAA time series at Mauna Loa has been subtracted from all data, since the HIPPO deployments spanned several years over a period when atmospheric N_2O was increasing by about 0.9 ppb/yr. HIPPO data extend up to 12-14 km and provide a fuller perspective with respect to altitude than the NOAA data in Figures 4-5 of the stratospheric influence on tropospheric N_2O.

3.2 Interannual variability in the seasonal N_2O minimum

In the SH, polar lower stratospheric temperature (PLST) from the previous spring is significantly negatively correlated to NOAA surface station N_2O monthly anomalies in austral summertime (January and February), when N_2O is descending into its autumn seasonal minimum. This correlation is observed at several extratropical southern NOAA sites including Cape Grim, Tasmania (CGO), Palmer Station, Antarctica (PSA) and South Pole (SPO) (Figure 7). The sign of the correlation is such that more negative surface N_2O anomalies occur during warm years, in which stronger than average descent of air depleted in N_2O occurs into the polar lower stratosphere over the austral winter and spring. Similar correlations are observed between GEOSCCM PLST and austral summer N_2O anomalies at these sites, although they are strongest in February and March, i.e., delayed by about 1 month relative to NOAA surface observations (Figure 7). In support of the observed surface correlations, altitude-latitude contour plots of QCLS aircraft data suggest more depleted N_2O values in the extratropical SH in February 2017 during ATom compared to ORCAS in February 2016, with the full global span of data in ATom-2 indicating a stratospheric influence originating from the southern polar region (Figure 8). The ORCAS aircraft campaign took place after

https://doi.org/10.5194/egusphere-2023-2877
Preprint. Discussion started: 8 December 2023

a particularly cold lower stratosphere Antarctic spring (weak Brewer Dobson circulation) while the ATom-2 deployment took place after a relatively warm spring (strong Brewer Dobson circulation).

In the NH in contrast, PLST from the previous winter is not correlated significantly to N_2O monthly anomalies at extratropical NOAA surface sites, either in August, the month of the seasonal minimum, nor in June and July, when N_2O is descending into its seasonal minimum. GEOSCCM also does not predict significant correlations between PLST and summer N_2O anomalies at most northern NOAA sites, with the exception of Mace Head, Ireland (MHD), where a negative correlation is found in July at MHD for both N_2O (R=-0.72) and N_2O_{ST} (R=-0.78) (Supplementary Figure S2).

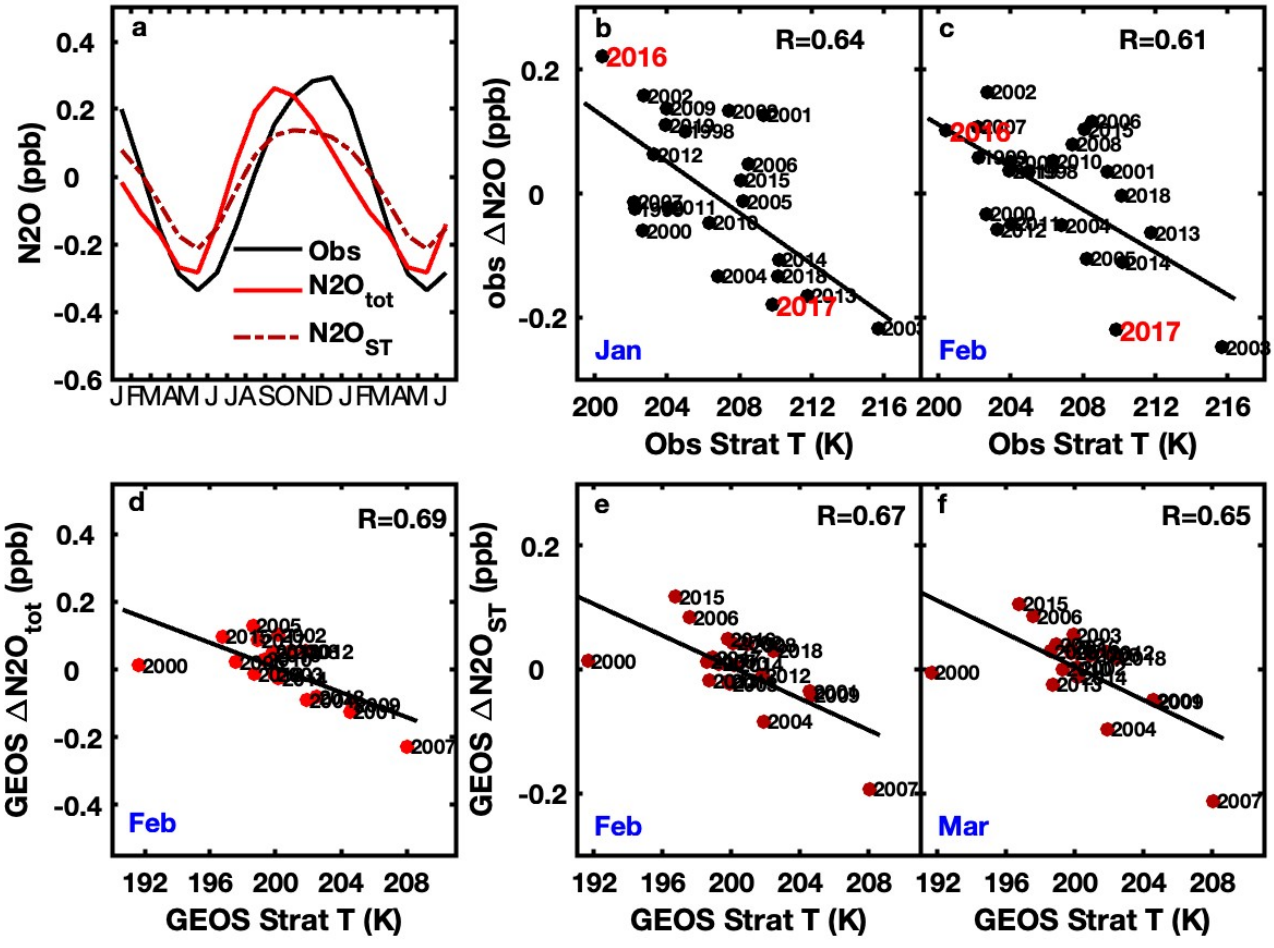

Figure 7: a) South Pole mean seasonal cycle in N_2O for observed N_2O and GEOSCCM total N_2O and N_2O_{ST}. NOAA surface N_2O seasonal anomalies in b) January and c) February at South Pole spanning 1997-2020, plotted vs. mean lower stratospheric MERRA-2 temperature at 100 hPa averaged over 60-90°S over the previous spring (September-November). The labeled anomalies in 2016 and 2017 correspond to the year of the ORCAS and ATom-2 aircraft campaigns, respectively. Bottom row shows GEOSCCM seasonal anomalies at South Pole spanning 2000-2019 for d) total N_2O in February and N_2O_{ST} in e) February and f) March plotted

https://doi.org/10.5194/egusphere-2023-2877
Preprint. Discussion started: 8 December 2023

vs. mean GEOSCCM lower stratospheric temperature at 100 hPa averaged over 60-90°S over the previous spring. The correlations between surface N_2O and stratospheric temperature are strongest for NOAA N_2O in January and February (austral summer), and for GEOSCCM N_2O in February and March, when N_2O is descending into its seasonal minimum.

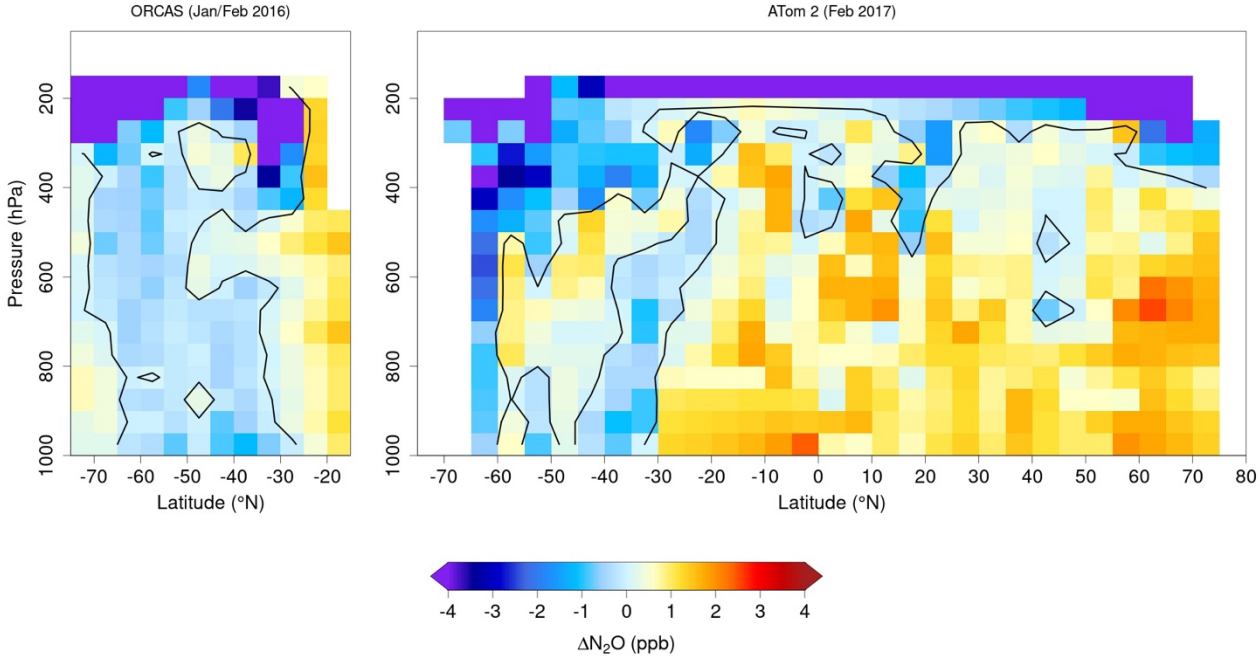

Figure 8. The 2 panels compare ORCAS (Jan.-Feb. 2016) and ATom-2 (Jan.-Feb. 2017) N_2O in ppb as a function of altitude and latitude, with interpolation and deseasonalizing the same as Figure 6. The ATom plot uses only the southbound portion of ATom-2. The comparison supports a stronger stratospheric influence during ATom-2 (a year of strong Brewer-Dobson circulation) than during ORCAS (a year of weak Brewer-Dobson circulation), as indicated in Figure 7b,c. The right panel shows ATom-2 data over the full 65°S to 75°N latitude span, putting the stratospheric influence coming from the southern polar stratosphere into broader perspective.

3.3 Interannual Variability in the Atmospheric Growth Rate (AGR) of Surface N_2O

The QBO index is positively correlated to the NOAA surface N_2O AGR in the SH, with an optimal correlation (R = 0.42) for QBO in the upper stratosphere at 20 hPa with a time shift of about 19 (17-21) months relative to the N_2O time series (Figure 9a). The correlation between GEOSCCM QBO and N_2O AGR in the SH is weak (R = 0.24) but also positive in sign in the upper stratosphere with a similar optimal shift in the GEOSCCM QBO of about 19 months (Figure 9c).

https://doi.org/10.5194/egusphere-2023-2877
Preprint. Discussion started: 8 December 2023

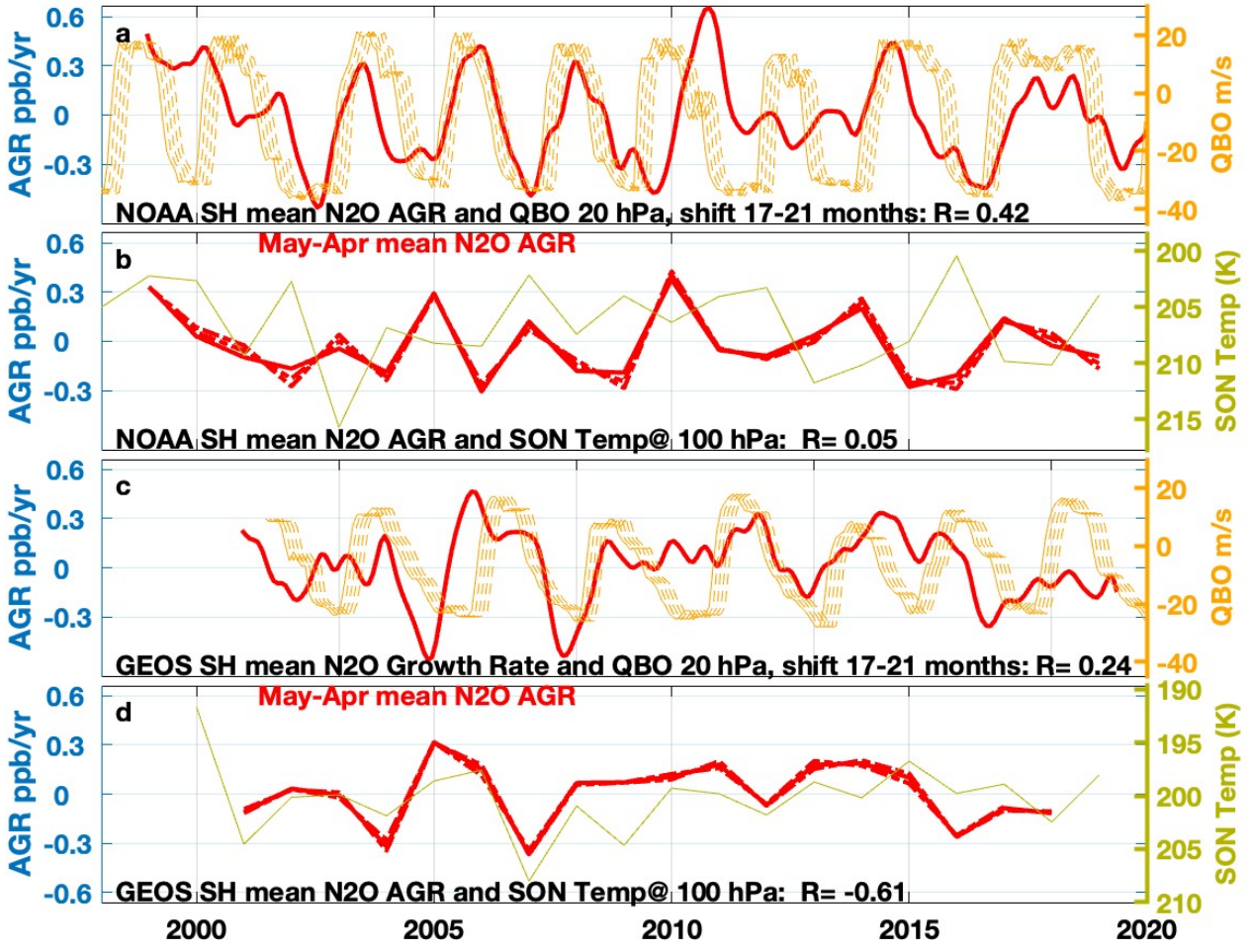

345 **Figure 9: (a,c) Southern hemisphere N_2O atmospheric growth rate (AGR) for NOAA (a) and GEOSCCM (c) plotted with the QBO index at 20 hPa with a 17-21 month forward shift in the index. (b,d) SH N_2O AGR plotted with mean lower stratospheric temperature averaged over 60-90°S for September-November in the year prior to the annual label on the X axis. The AGR is averaged from monthly N_2O data over the ensuing 12 month period May-April (solid red line), shifted plus or minus 1 month (dotted red lines), for NOAA (b) and GEOSCCM (d). Note: to convert to %/yr (AGR units often used in the literature) ppb/yr can be**
350 **multiplied by 100/323 (~1/3), where 323 is the mean tropospheric mixing ratio of N_2O over 1999-2020.**

In contrast to the SH, the NOAA surface N_2O AGR in the NH is negative in sign and not significantly correlated to the QBO index at any altitude. The strongest of the weak correlations in the NH occurs for 50 hPa QBO (R=-0.23) with a 10-14 months lag (Figure 10a). GEOSCCM predicts a significant negative correlation (R = -0.47) between the GEOSCCM QBO and the
355 NH N_2O AGR, which also is optimal around 50 hPa with 10-14 month QBO lag (Figure 10c).

https://doi.org/10.5194/egusphere-2023-2877
Preprint. Discussion started: 8 December 2023

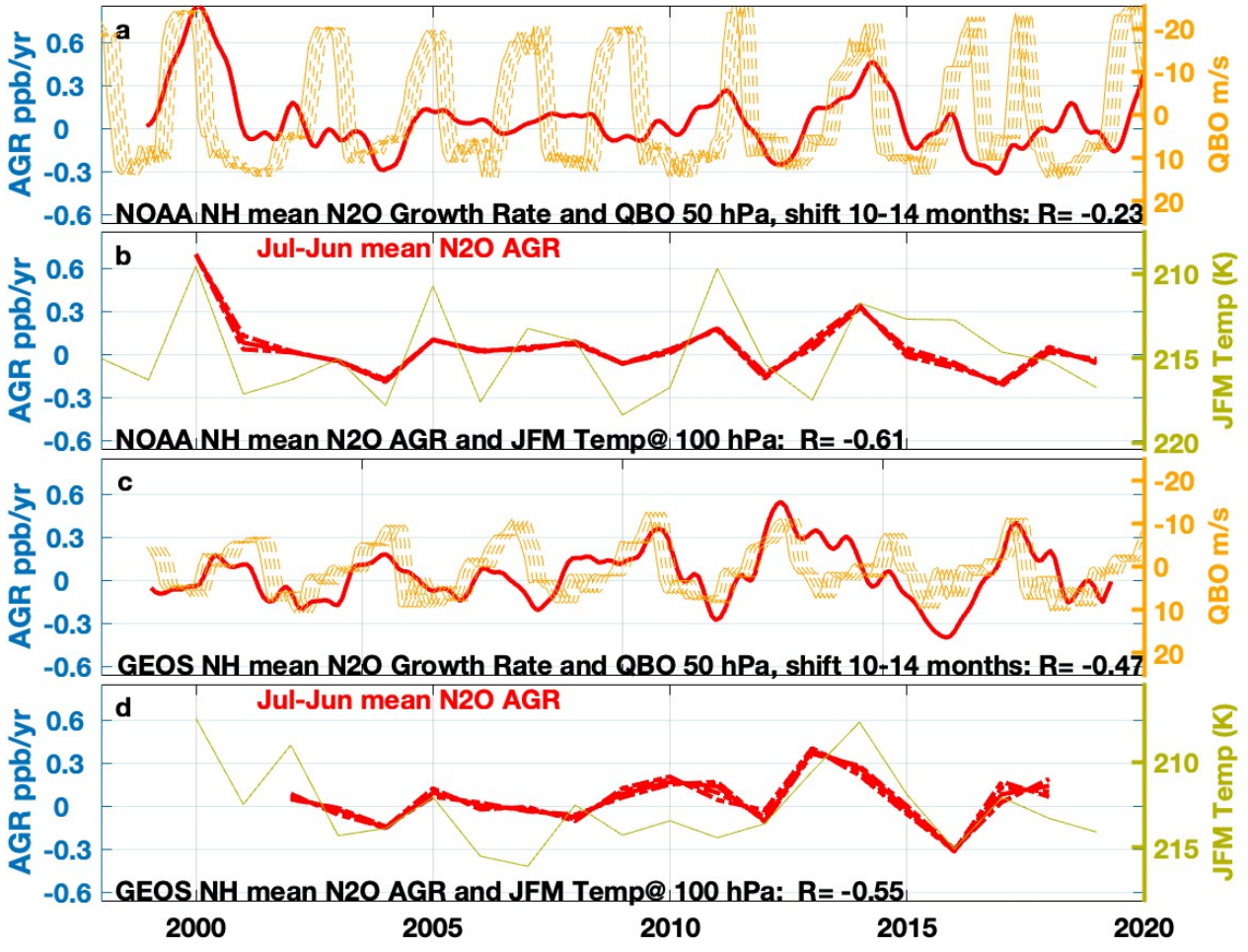

Figure 10: (a,c) Northern hemisphere N_2O atmospheric growth rate (AGR) for NOAA (a) and GEOS (c) plotted with the QBO index at 50 hPa with a 10-14 month forward shift in the index. (b,d) NH N_2O AGR plotted with mean lower stratospheric temperature averaged over 60-90°N over January-March of the year labeled on each data point. The AGR is averaged from monthly N_2O data over the encompassing 12 month period July-June (solid red line), shifted plus or minus 1 month (dotted red lines), for NOAA (b) and GEOSCCM (d).

In the SH, PLST is not significantly correlated to the surface N_2O AGR observed by NOAA, but within GEOSCCM the two are negatively correlated (Figure 9b,d). The correlation with PLST in GEOSCCM occurs for the N_2O AGR averaged over a wide range of 12-month intervals extending from November-October, overlapping with and proceeding the September-November PLST average, through the following August-July, with the strongest correlation (R = -0.61) over May-April.

In the NH, winter PLST is negatively correlated to the NOAA surface N_2O AGR (R = -0.61) with an optimal correlation for the 12 month period of July-June encompassing the January-March PLST average (Figure 10b). A similar correlation is found

https://doi.org/10.5194/egusphere-2023-2877
Preprint. Discussion started: 8 December 2023

between the GEOSCCM PLST and the N_2O AGR in the NH (Figure 10d).

The Niño 3.4 index is negatively correlated (R = -0.5) to the NOAA surface N_2O AGR both globally and in the SH, with little to no monthly lag in the index. In the NH, the correlation is weaker (R=-0.35) with an optimal lag of 7 months in the Niño 3.4 index relative to the NOAA N_2O AGR (Figure 11).

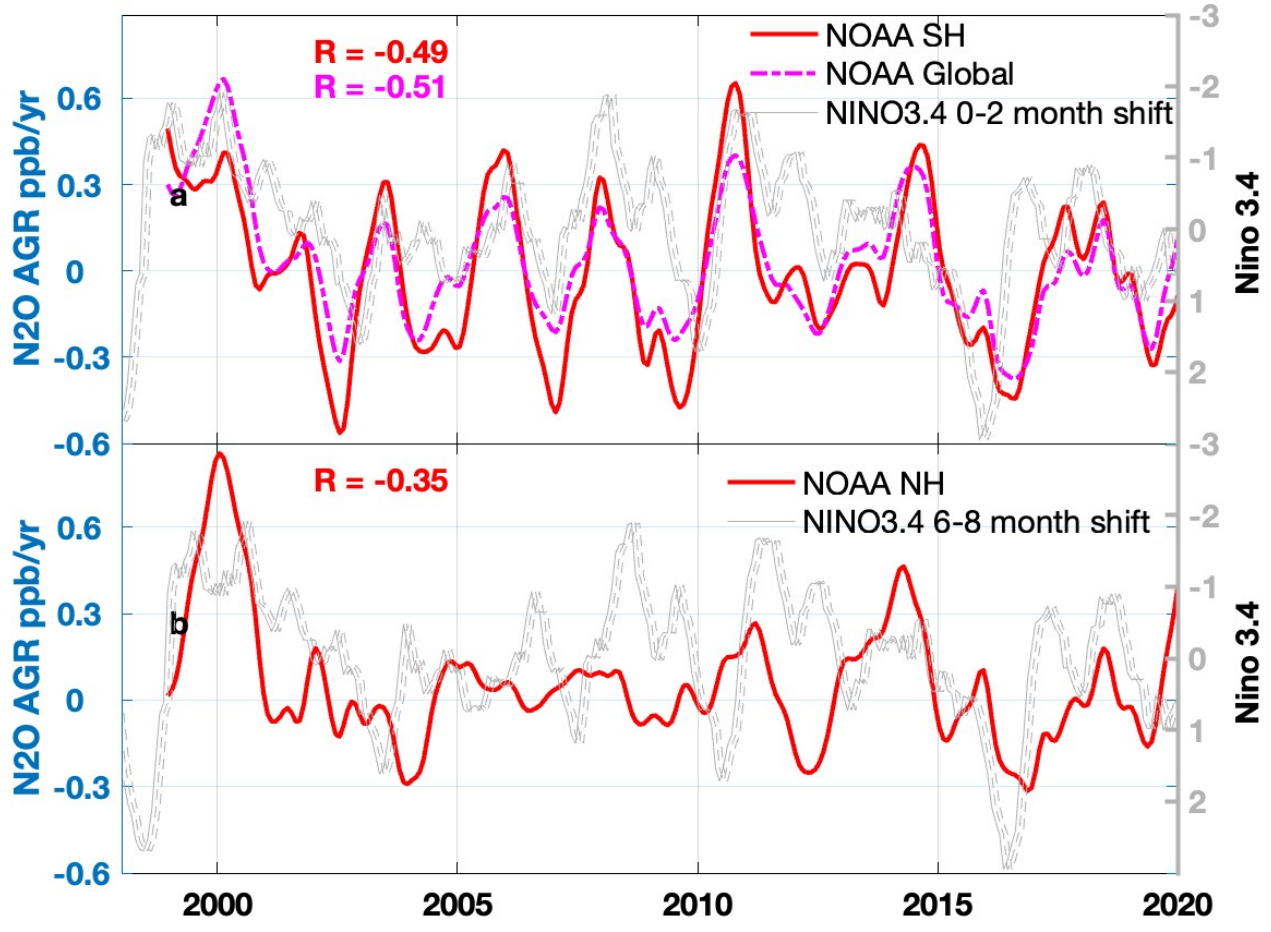

Figure 11: NOAA N_2O AGR plotted with the Nino3.4 index for a) SH and global mean AGR with a 0-2 month shift in the index and b) NH AGR with a 6-8 month shift in the index.

4. Discussion

Both the model results and the NOAA surface station and QCLS aircraft observations presented here suggest that the stratosphere helps drive the seasonal minimum in tropospheric N_2O and also influences its atmospheric growth rate. Multiple lines of evidence point to this conclusion. First, vertical profiles of atmospheric N_2O from aircraft provide a new, big picture perspective, in which N_2O-depleted air originates in the winter polar lower stratosphere, crosses the tropopause in spring or

https://doi.org/10.5194/egusphere-2023-2877
Preprint. Discussion started: 8 December 2023

early summer around the time of vortex breakup, and descends downward and equatorward, reaching Earth's surface by summer or early fall. Second, PLST and QBO indices correlate significantly to the surface N_2O AGR in the NH and SH, respectively. PLST also correlates with monthly anomalies at or near the time of the seasonal minimum in the SH. These correlations are consistent with a stronger stratospheric influence in years with a stronger Brewer Dobson circulation and are similar to correlations found in previous studies (*Nevison et al.*, 2007; 2011). Finally, GEOSCCM simulations with an explicitly resolved stratospheric N_2O tracer yield similar N_2O AGR correlations with internally modeled QBO and PLST indices, and show similar 3-dimensional patterns to those in the NOAA empirical background and in QCLS aircraft data, although with some differences in phasing and propagation time of the stratospheric signal to the surface.

4.1 The Brewer Dobson circulation

The mechanistic pathway by which the stratosphere imparts a distinct seasonal signature to surface N_2O is linked to the Brewer Dobson circulation (BDC), which transports warm, N_2O-depleted air from the middle and upper stratosphere into the polar lower stratosphere in the winter hemisphere (*Holton et al.*, 1995; *Liang et al.*, 2008; 2009; *Nevison et al.*, 2011; *Butchart*, 2014). This wintertime descent leads to a large seasonal amplitude in the polar lower stratosphere, in which the N_2O mixing ratio reaches its minimum in spring just before the time of polar vortex break-up. N_2O-depleted air is brought into the troposphere by slow diabatic descent and mixing across the polar tropopause as well as entrainment due to the summertime increase in tropopause height. This air is then mixed between the mid and high latitudes via various synoptic-scale eddies in extra-tropical cyclones (*Stohl et al.*, 2001). The cross-tropopause gradient between the spring polar lower stratosphere and the troposphere can be 50 ppb or more but stratospheric air is strongly diluted after it enters the troposphere. By the time the stratospheric depletion signal propagates down to the lower troposphere it is reduced by a factor of ~100, contributing to the < 1 ppb seasonal amplitude observed in N_2O at surface sites (*Nevison et al.*, 2004; 2011; *Liang et al.*, 2009).

4.2 The QBO and its relationship with the Brewer Dobson circulation

The QBO is the primary mode of variability governing the amount of N_2O that upwells from the tropical lower stratosphere into the middle and upper tropical stratosphere, the region of peak photochemical destruction (*Baldwin et al.*, 2001; *Prather et al.*, 2015; *Ruiz et al.,* 2021). Photochemical destruction is highest when QBO winds at higher altitudes (~30 hPa and above) are in the westerly (positive) phase and lower altitude QBO winds are in the easterly (negative) phase. This configuration is associated with increased vertical upwelling in the tropical lower stratosphere, which transports more N_2O to its peak loss region (~32 km) (*Strahan et al.*, 2021; *Ruiz et al.*, 2021).

In addition to the primary vertical circulation, the QBO has an associated secondary or meridional circulation, which in the SH involves transport of photochemically-depleted tropical air into the subtropical middle stratosphere followed by planetary wave-driven mixing, which homogenizes this air over a broad area known as the "surf zone" (*Strahan et al.*, 2015). The surf

https://doi.org/10.5194/egusphere-2023-2877
Preprint. Discussion started: 8 December 2023

zone extends from about 30 hPa to 10 hPa in altitude and 15-70º S in latitude. Paradoxically, in the positive QBO phase in the upper stratosphere, when the N_2O photochemical loss is at its peak, relatively less N_2O-depleted air enters the subtropical surf zone, due to the upward/clockwise flow of the secondary QBO circulation (*Strahan et al.*, 2015).

N_2O-depleted air in the surf zone (set by the QBO) subsequently is mixed into the polar region during the late spring breakup of the Antarctic polar vortex and summer-to-fall SH vortex development. The N_2O anomaly is then set into the Antarctic region as the polar vortex forms in the fall. The vortex-trapped N_2O anomaly undergoes diabatic descent, driven by the BDC and in isolation from mixing with lower latitudes, through the fall and winter (*Rosenfield et al.,* 1994). After a few winter months of BDC-driven diabatic descent, the anomaly arrives in the Antarctic lower stratosphere in the July-September period, about 1 year after it formed in the middle tropical stratosphere (*Strahan et al.*, 2015). Continued descent and mixing across the polar tropopause bring the N_2O depleted air down to the surface ~4 months later, consistent with the long (17-19 month) delay between the QBO index at 20 hPa and the surface SH N_2O AGR anomalies in NOAA surface station data found in our analysis (Figure 9).

The strong isolation of the Antarctic polar vortex prevents mixing with midlatitudes during the period of diabatic descent from the altitude of the "surf zone" and is consistent with our finding that significant correlations with the NOAA surface N_2O AGR in the SH occur mainly for higher altitude QBO indices between about 30 and 10 hPa. The positive sign of the N_2O AGR correlation with the QBO index at those altitudes may be explained by the fact that the QBO meridional circulation brings relatively less N_2O depleted air into the subtropical surf zone during the phase when the QBO is positive (westerly winds) in the upper tropical stratosphere above about 30 hPa (*Strahan et al.*, 2015). This leads to a positive N_2O anomaly (i.e., photochemically depleted, but less depleted than average) in the surf zone that ultimately is mixed into the polar region and transported into the troposphere via diabatic descent and mixing. When this signal of relatively low N_2O depletion is felt at Earth's surface, it permits a more positive N_2O AGR than normal, hence the positive correlation with the positive (westerly) QBO at 10-30 hPa that originally drove the stratospheric N_2O anomaly well over a year prior.

The dynamics of the QBO, its interaction with the BDC and ultimate influence on surface N_2O are complex, as described above. The QBO-associated photochemical destruction anomaly per se is not the main determinant of the stratospheric influence on surface N_2O, since one would otherwise expect a negative correlation between the upper altitude QBO and the surface N_2O AGR instead of the positive correlation found in Figure 9. *Ruiz et al.* (2021) similarly concluded that surface variability in N_2O is not correlated directly to the QBO-driven variability in stratospheric loss, but rather by dynamical variations in cross tropopause fluxes of air, which are governed at least in part by the BDC.

Like our study, *Ray et al.* (2020) found a positive correlation between the QBO index at 50 hPa and the NOAA surface N_2O AGR in the SH (but not the NH). Their QBO index was somewhat lower in altitude than our optimally selected altitude (20

https://doi.org/10.5194/egusphere-2023-2877
Preprint. Discussion started: 8 December 2023

hPa) and their optimal phase shift was somewhat less (8-12 months) than our optimal 19 month phase shift. This was likely a result of the time lag in the downward propagation of the QBO winds. Our own correlation analysis across a range of altitudes shows a positive correlation between QBO and the SH N_2O AGR in which the correlation weakens and the optimal lag time decreases with decreasing altitude (Supplementary Figure S3). At 50 hPa, we find an optimal lag time of 10-12 months (R = 0.33), consistent with *Ray et al.* (2020).

4.3 Northern vs. southern hemisphere differences

In the NH, some of the same mechanisms and interactions between the QBO and BDC occur, but they are more difficult to isolate than in the SH due to the more complex atmospheric dynamics of the NH stratosphere. The deposition of momentum from planetary scale Rossby waves propagating into the stratosphere is the fundamental driver of the BDC. *Holton and Tan* (1980) originally showed that a deep and cold northern winter polar vortex was associated with the QBO westerly phase, and a weaker and warmer vortex associated with the easterly phase. Hence, the year-to-year integrated strength of the BDC is tied to the interaction of the NH mean flow with the QBO. Further, the BDC strength and structure is also tied to meridional mixing of air. In addition to the QBO influence on the northern polar vortex, the QBO induces a meridional circulation that directly impacts the northern mid-latitudes (e.g., *Randel and Wu*, 1996). The NH mid-winter QBO and wave mean-flow interaction has two effects: 1) it modulates the strength and structure of the BDC, and 2) it also modifies mixing between the Arctic polar vortex and the northern mid-latitudes by Rossby waves. These complex dynamics may explain why the N_2O AGR at NH sites correlates best with lower stratosphere QBO indices, why they have a negative rather than positive sign (due to the vertical reversal of the sign of QBO with altitude https://acd-ext.gsfc.nasa.gov/Data_services/met/qbo/qbo.html) and why these correlations are generally weaker than at southern sites.

In the NH, both NOAA surface stations and GEOSCCM show a significant negative correlation between PLST and the N_2O AGR, which is consistent with a slower N_2O growth rate during years with a stronger BDC. The planetary wave activity that drives the BDC is strongest in the NH due to the more variable topography and stronger land-sea contrasts in the NH compared to the SH. Thus the BDC-driven descent into the winter pole is more strongly seasonal in the NH than in the SH (*Holton et al.*, 1995). For both NOAA surface stations and GEOSCCM, the NH N_2O AGR is more strongly correlated to PLST than it is to the QBO, suggesting the stronger proximal influence of the BDC and stratosphere-troposphere exchange on the AGR, consistent with *Ruiz et al.* (2021). The weak, statistically insignificant correlation between QBO and NOAA surface N_2O AGR is consistent with the results of *Ray et al.* (2020) and the complex dynamical interactions between the BDC and the QBO in the NH discussed above.

In contrast to the NH, the NOAA SH surface N_2O AGR does not correlate to PLST but does correlate to QBO. This result is somewhat puzzling, especially given the significant correlation between PLST and NOAA surface station N_2O monthly

https://doi.org/10.5194/egusphere-2023-2877
Preprint. Discussion started: 8 December 2023

anomalies in January and February (Figure 7), which are corroborated by the ATom-2 and ORCAS data (Figure 8). It appears that the impact of the stratosphere in austral summer as tropospheric N_2O descends into its seasonal minimum is not sufficient to influence the SH N_2O AGR over a full 12-month period.

The SH N_2O AGR results may reflect the strong preservation of the surf zone QBO signal that mixes into the polar region and is ultimately transported into the troposphere as per *Strahan et al.* (2015) combined with the relatively weaker BDC in the SH and/or the interference of ENSO-driven signals discussed below. The fact that PLST does correlate with the SH N_2O AGR in GEOSCCM output suggests that GEOSCCM may overestimate the influence of the BDC in the SH or that the correlation may be cleaner due to the lack of a competing ENSO influence in GEOSCCM.

4.4 Correlations with ENSO

The NOAA surface station N_2O AGR correlation with ENSO indices is similar in magnitude to the correlations with stratospheric indices in the SH (R = -0.49, 0-2 month phase shift) and relatively weaker in the NH (R=-0.35, 7 month optimal phase shift) (Figure 10). The correlation in the SH could in part reflect meteorological shifts in the tropical low level convergence pattern during positive ENSO (El Niño) conditions. For atmospheric gases with a positive north-south latitudinal gradient, these shifts result in a lessened influence of winds from the NH on the tropical SH, e.g., at the NOAA Samoa site, and a heightened influence of southeasterly winds (*Prinn et al.*, 1992; *Nevison et al.*, 2007). The fact that the N_2O AGR correlation with ENSO is considerably weaker in the NH than in the SH suggests a limited impact of ENSO on NH N_2O and supports the hypothesis that reduced north-to-south transport during El Niño phases contributes to the correlation observed in the SH.

The negative correlation between N_2O AGR and ENSO also may reflect a true reduction in the biogeochemical N_2O source during the positive ENSO phase, for example, due to drought over tropical land or due to reduced upwelling in the tropical ocean (*Ishijima et al.*, 2009; *Thompson et al.*, 2013). The most well documented biogeochemical response of N_2O to ENSO events occurs in the Eastern Tropical South Pacific (ETSP), a well known oxygen minimum zone (OMZ) and hot spot of oceanic N_2O emissions (*Arévalo-Martínez*, 2015; *Ji et al.*, 2019). El Niño conditions decrease upwelling in the ETSP, thereby reducing the surface productivity, deepening the oxycline, contracting the OMZ and decreasing the N_2O sea-to-air flux (*Ji et al.*, 2019; *Babbin et al.*, 2015).

However, it is likely that less than one quarter of the total N_2O budget comes from oceanic emissions, of which the ETSP is only one component (*Yang et al.*, 2020; *Canadell et al.*, 2021). This raises questions about whether a reduced ETSP source has enough leverage to control the overall N_2O AGR. *Ruiz et al.* (2021) removed the stratospheric influence from surface N_2O data to tease out a source of ~ 1 Tg N (about 5% of the total annual N_2O source) associated with the 2010 La Niña

https://doi.org/10.5194/egusphere-2023-2877
Preprint. Discussion started: 8 December 2023

event, which could have come from tropical land or ocean, or some combination of both. Similarly, *Kort et al.* (2011) found evidence of strong episodic pulses of ~ 1 Tg N from tropical regions, based on maxima in QCLS N_2O data measured in the middle and upper troposphere during aircraft campaigns in 2009. These pulses were not tied specifically to an ENSO event but rather more generally provided a testament to the strength of the tropical N_2O source.

The 1 Tg N La Niña source inferred by Ruiz *et al.* (2021) raises the possibility that both ENSO and the stratosphere may jointly influence the N_2O AGR, in a manner that may complicate single variable correlation analyses. Consistent with this hypothesis, in our own study, a multivariate correlation of both QBO at 20 hPa with 19 month lag and the Niño 3.4 index with 0 months lag better captures the variability in the SH N_2O AGR ($R = 0.61$) than either index alone ($R = 0.42$ and -0.49, respectively).

5 Conclusions

Global airborne surveys provide new insights into stratospheric influences on tropospheric N_2O and advance our ability to understand surface variability in N_2O sources. N_2O observations from these surveys support GEOSCCM simulations in showing that N_2O-depleted air accumulates throughout the winter in the polar lower stratosphere, crosses the polar tropopause in spring or early summer, and descends downward and equatorward, transmitting a coherent signal to Earth's surface in the summer to early-autumn period. In support of this view, significant correlations are found between the N_2O AGR observed at long-term surface monitoring sites and either the QBO index in the SH or PLST in the NH, where PLST is a proxy for the strength of the BDC. Correlations between the N_2O AGR and ENSO indices are also significant in the SH, suggesting a joint influence of ENSO and the stratosphere on the AGR in that hemisphere. The QBO influences the rate at which N_2O is delivered to and destroyed in the tropical middle to upper stratosphere, but complex atmospheric dynamics buffer how variations in the stratospheric N_2O loss rate are transmitted across the tropopause to modulate the surface N_2O AGR. Stratosphere-troposphere exchange in polar regions is linked closely to the BDC and appears to be a more direct influence than the QBO on the N_2O AGR in the NH. In contrast, in the SH, the combination of a better-preserved QBO signal and weaker BDC may lead to a direct (albeit with a ~1.5 year lag) correlation between the QBO and the SH N_2O surface AGR, consistent with our understanding of stratospheric dynamics.

Code Availability

Codes are available from the corresponding author upon request.

Data Availability

NOAA N_2O data can be obtained by contacting xin.lan@noaa.gov or through the NOAA Global Monitoring Laboratory at https://gml.noaa.gov/aftp/data/trace_gases/n2o/flask/. QCLS N_2O data are openly available and archived in the Oak Ridge National Laboratory Distributed Active Archive Center (ORNL DAAC) https://doi.org/10.3334/ORNLDAAC/1925 (ATom),

https://doi.org/10.5194/egusphere-2023-2877
Preprint. Discussion started: 8 December 2023

and at the National Center for Atmospheric Research (NCAR) https://doi.org/10.5065/D6SB445X (ORCAS) and https://doi.org/10.3334/CDIAC/HIPPO_010 (HIPPO).

Author contributions

CDN designed and carried out the analysis and prepared the main manuscript and most of the figures. QL implemented separate stratospheric and tropospheric N_2O tracers in GEOSCCM and provided model output. PN computed QBO indices and MERRA stratospheric temperatures and provided guidance on stratospheric dynamics. BBS, RC, YG and EK provided QCLS N_2O data and BBS created contour plots of the QCLS data. XL and GD provided N_2O surface data. All authors reviewed and approved the manuscript.

Competing Interests

The authors declare they have no conflicts of interest.

Acknowledgments

CDN and QL acknowledge support from the NASA MAPS program (award 16-MAP16-0049). The authors are grateful to Arlyn Andrews, Colm Sweeney, Bradley Hall, Ed Dlugokencky, Steve Wofsy, Bruce Daube, and many others who have made this study possible, through collection and analysis of surface station and NOAA aircraft flasks, in situ NOAA station measurements, and QCLS aircraft campaign observations. The HIPPO and ORCAS observations, and the contributions of BBS were supported by the National Center for Atmospheric Research, which is a major facility sponsored by the National Science Foundation under Cooperative Agreement No. 1852977.

References

Akima, H.: A Method of Bivariate Interpolation and Smooth Surface Fitting for Irregularly Distributed Data Points, ACM Transactions on Mathematical Software, Vol. 4, No. 2, June 1978, pp. 148-159. Copyright 1978, Association for Computing Machinery, Inc, 1978

Arévalo-Martínez, D. L., Kock, A., Löscher, C. R., Schmitz, R. A. & Bange, H. W.: Massive nitrous oxide emissions from the tropical South Pacific Ocean. Nat. Geosci., 8, 530, 2015.

Babbin, A.R., Bianchi, D., Jayakumar, A, and Ward, B. B.: Rapid nitrous oxide cycling in the suboxic ocean, Science, 348, doi:10.1126/science.aaa8380, 2015.

Baldwin, M.P., Gray, L.J., Dunkerton, T.J., Hamilton, K., Haynes, P.H., Randel, W.J., Holton, J.R., Alexander, M.J., Hirota, I., Horinouchi, T., Jones, D.B.A., Kinnersley, J.S., Marquardt, C., Sato, K., Takahashi, M., The quasi-biennial oscillation, Reviews of Geophysics, 39(2), 179-229, 2001.

https://doi.org/10.5194/egusphere-2023-2877
Preprint. Discussion started: 8 December 2023

Bouwman, A.F. and Taylor, J.A.: Testing high-resolution nitrous oxide emission estimates against observations using an atmospheric transport model, Global Biogeochem. Cy., 10, 307-318, 1996.

Bouwman, A.F., van der Hoek, K.W., and Olivier, J.G.J.: Uncertainties in the global source distribution of nitrous oxide, J. Geophys. Res., 100, 2785-2800, 1995.

Butchart, N.: Reviews of Geophysics The Brewer-Dobson circulation, Rev. Geophys, 52, 157–184. https://doi.org/10.1002/2013RG000448, 2014.

Canadell, J. G., P. M. S. Monteiro, M. H. Costa, L. Cotrim da Cunha, P. M. Cox, A. V. Eliseev, S. Henson, M. Ishii, S. Jaccard, C. Koven, A. Lohila, P. K. Patra, S. Piao, J. Rogelj, S. Syampungani, S. Zaehle, K. Zickfeld, 2021, Global Carbon and other Biogeochemical Cycles and Feedbacks. In: Climate Change 2021: The Physical Science Basis. Contribution of Working Group I to the Sixth Assessment Report of the Intergovernmental Panel on Climate Change (Masson-Delmotte, V., P. Zhai, A. Pirani, S. L. Connors, C. Péan, S. Berger, N. Caud, Y. Chen, L. Goldfarb, M. I. Gomis, M. Huang, K. Leitzell, E. Lonnoy, J.B.R. Matthews, T. K. Maycock, T. Waterfield, O. Yelekçi, R. Yu and B. Zhou (eds.)). Cambridge University Press. In Press.

Earth Systems Research Laboratory, Multivariate ENSO Index (MEI). NOAA (2017).

Elkins, J.W, and Dutton, G.S.: Nitrous oxide and sulfur hexafluoride (in 'State of the Climate in 2008'), Bull. Amer. Meteor. Soc, 90, S38-S39, 2009.

Forster, P., Ramaswamy, V., Artaxo, P., Berntsen, T., Betts, R., Fahey, D.W., Haywood, J., Lean, J., Lowe, D.C., Myhre, G., Nganga, J., Prinn, R., Raga, G., Schulz, M. and Van Dorland, R.: Changes in Atmospheric Constituents and in Radiative Forcing. In: Climate Change 2007: The Physical Science Basis. Contribution of Working Group I to the Fourth Assessment Report of the Intergovernmental Panel on Climate Change. Cambridge University Press Cambridge, United Kingdom and New York, NY, USA, 2007.

Glatthor, N., von Clarmann, T., Fischer, H., Funke, B., Grabowski, U., Hoepfner, M., Kellmann, S., Kiefer, M., Linden, A., Milz, M., Steck, T., Stiller, G.P., Mengistu Tsidu, G., Wang, D.-Y.: Mixing processes duing the Antarctic vortex split in September-October 2002 as inferred from source gas and ozone distributions from ENVISAT-MIPAS, J. Atmos. Sci., 62(3), 787-800, 2005.

Gonzalez, Y., Commane, R., Manninen, E., Daube, B.C., Schiferl, L., McManus, J.B., McKain, K, Hintsa, E.J., Elkins, J.W., Montzka, S.A., Impact of stratospheric air and surface emissions on tropospheric nitrous oxide during ATom, Atmospheric Chemistry and Physics Discussions, https://doi.org/10.5194/acp-2021-167, 2021.

Gurney, K. R., Law, R.M., Denning, A.S., Rayner, P.J., Pak, B.C., Baker, D.F., Bousquet, P., Bruhwiler, L., Chen, Y.-H., Ciais, P., Fung, I.Y., Heimann, M., John, J., Maki, T., Maksyutov, S., Peylin, P., Prather, M., Taguchi, S.: Transcom 3 inversion intercomparison: Model mean results for the estimation of seasonal carbon sources and sinks, Global Biogeochem. Cycles, 18, GB1010, doi:10.1029/2003GB002111, 2004.

Hall, B. D., Dutton, G.S., and Elkins, J. W.: The NOAA nitrous oxide standard scale for atmospheric observations, J. Geophys. Res., 112, D09305, doi:10.1029/2006JD007954, 2007.

https://doi.org/10.5194/egusphere-2023-2877
Preprint. Discussion started: 8 December 2023

Hall, B. D., Dutton, G. S., Mondeel, D. J., Nance, J. D., Rigby, M., Butler, J. H., Moore, F. L., Hurst, D. F. and Elkins, J. W.: Improving measurements of SF_6 for the study of atmospheric transport and emissions, Atmos. Meas. Tech., 4, 2441-2451, doi: 10.5194/amt-4-2441-2011, 2011.

Hammerling, D. M., Michalak, A. M., Kawa, S. R.: Mapping of CO_2 at High Spatiotemporal Resolution using Satellite Observations: Global Distributions from OCO-2, Journal of Geophysical Research, 117, D06306, doi:10.1029/2011JD017015, 2012.

Hirsch, A.I., Michalak, A.M., Bruhwiler, L.M., Peters, W., Dlugokencky, E.J. and Tans, P.P.: Inverse modeling estimates of the global nitrous oxide surface flux from 1998-2001, Global Biogeochem. Cy., 20, GB1008, doi:10.1029/2004GB002443, 2006.

Holton, J.R., Haynes, P.H., McIntyre, M.E., Douglass, A.R., Rood, R.B. and Pfister, L.: Stratosphere-troposphere exchange, Rev. Geophys., 33(4), 403-439, 1995.

Huang, J., Golombek, A., Prinn, R., Weiss, R., Fraser, P., Simmonds, P., Dlugokencky, E.J., Hall, B., Elkins, J., Steele, P., Langenfelds, R., Krummel, P., Dutton, G., and Porter, L.: Estimation of regional emissions of nitrous oxide from 1997 to 2005 using multinetwork measurements, a chemical transport model, and an inverse method, J. Geophys. Res. 113, D17313, doi:10.1029/2007JD009381, 2008.

Ishijima, K., Patra, P.K., Takigawa, M., Machida, T., Matsueda, H., Sawa, Y., Steele, L.P., Krummel, P.B., Langenfelds, R.L., Aoki, S. and Nakazawa, T.: The stratospheric influence on the seasonal cycle of nitrous oxide in the troposphere as deduced from aircraft observations and model simulations, J. Geophys. Res., 115, D20308, doi:10.1029/2009JD013322, 2010.

Ji, Q., Babbin, A.R., Jayakumar, A., Oleynik, S. and Ward, BB.: 2015: Nitrous oxide production by nitrification and denitrification in the Eastern Tropical South Pacific oxygen minimum zone. Geophysical Research Letters, 42(24), 10,755–10,764, doi:10.1002/2015gl066853.

Ji, Q. et al.: Investigating the effect of El Niño on nitrous oxide distribution in the eastern tropical South Pacific. Biogeosciences, 16(9), 2079–2093, doi:10.5194/bg-16-2079-2019, 2019.

Jiang, X, Ku, W.L., Shia, R.-L., Li, Q., Elkins, J.W., Prinn, R.G., Yung, Y.L.: Seasonal cycle of N_2O: Analysis of data, Global Biogeochem. Cy., 21, GB1006, doi:10.1029/2006GB002691, 2007.

Jin, X. and Gruber, N.: Offsetting the radiative benefit of ocean iron fertilization by enhancing N_2O emissions, Geophys. Res. Lett. 30(24), 2249, 2003.

Jin, X., Najjar, R.G., Louanchi, F., and Doney, S.C.: A modeling study of the seasonal oxygen budget of the global ocean, J. Geophys. Res., 112, C05017, doi:10.1029/2006JC003731, 2007.

Kalnay, E., Kanamitsu, M., Kistler, R., Collins, W., Deaven, D., Gandin, L., Iredell, M., Saha, S., White, G., Woollen, J., Zhu, Y., Leetmaa, A., Reynolds, R., Chelliah, M., Ebisuzaki, W., Higgins, W., Janowiak, J., Mo, K.C., Ropelewski, C., Wang, J., Jenne, R., Joseph, D.: The NMC/NCAR 40-year reanalysis project, B. Am. Meteorol. Soc., 77, 437– 471, 1996.

Khosrawi, F., Mueller, R. Proffitt, M. H., Urban, J., Murtagh, D., Ruhnke, R. Grooß, J.-U. and Nakajima, H.: Seasonal cycle of averages of nitrous oxide and ozone in the Northern and Southern Hemisphere polar, midlatitude, and tropical regions

https://doi.org/10.5194/egusphere-2023-2877
Preprint. Discussion started: 8 December 2023

derived from ILAS/ILAS-II and Odin/SMR observations, J. Geophys. Res., 113, D18305, doi:10.1029/2007JD009556, 2008.

Kort, E. A., Patra, P. K., Ishijima, K., Daube, B. C., Jiménez, R., Elkins, J.W., Hurst, D., Moore, F. L., Sweeney, C. and Wofsy, S. C.: Tropospheric distri- bution and variability of N_2O: Evidence for strong tropical emissions, Geophys. Res. Lett., 38, L15806, doi:10.1029/2011GL047612, 2011.

Kroeze, C., Mosier, A. and Bouwman, L.: Closing the global N_2O budget: A retrospective analysis 1500-1994, Global Biogeochemical Cycles, 13, 1-8, 1999.

Lambert, A., Read, W. G., Livesey, N. J., Santee, M.L., Manney, G.L., Froidevaux, L., Wu, D.L., Schwartz, M.J., Pumphrey, H.C., Jimenez, C., Nedoluha, G.E., Cofield, R.E., Cuddy, D.T., Daffer, W.H., Drouin, B.J., Fuller, R.A., Jarnot, R.F., Knosp, B.W., Pickett, H.M., Perun, V.S., Snyder, W.V., Stek, P.C., Thurstans, R.P., Wagner, P.A., Waters, J.W., Jucks, K.W., Toon, G.C., Stachnik, R.A., Bernath, P.F., Boone, C.D., Walker, K.A., Urban, J., Murtagh, D., Elkins, J.W., Atlas, E.: Validation of the Aura Microwave LihPa Sounder middle atmosphere water vapor and nitrous oxide measurements, J. Geophys. Res., 112, D24S36, doi:10.1029/2007JD008724, 2007.

Lan, X., Dlugokencky, E.J., Mund, J.W., Crotwell, A.M., Crotwell, M.J., Moglia, E., Madronich, M., Neff, D. and Thoning, K.W.: Atmospheric Nitrous Oxide Dry Air Mole Fractions from the NOAA GML Carbon Cycle Cooperative Global Air Sampling Network, 1997-2021, Version: 2022-11-21, https://doi.org/10.15138/53g1-x417, 2022.

Lan, X., Tans, P., Thoning, K., & NOAA Global Monitoring Laboratory. (2023). NOAA Greenhouse Gas Marine Boundary Layer Reference - N2O. (Data set). NOAA GML. https://doi.org/10.15138/83W5-DK71.

Liang, Q., Stolarski, R.S., Douglass, A.R., Newman, P.A. and Nielsen, J.E.: Evaluation of emissions and transport of CFCs using surface observations and their seasonal cycles and the GEOS CCM simulation with emissions-based forcing, J. Geophys. Res., 113, D14302, doi:10.1029/2007JD009617, 2008.

Liang, Q., Douglass, A.R., Duncan, B.N., Stolarski, R.S. and Witte, J.C.: The governing processes and timescales of stratosphere-to-troposphere transport and its contribution to ozone in the Arctic troposphere, Atmos. Chem. Phys., 9, 3011-3025, 2009.

Liang, Q., Nevison, C., Dlugokencky, E., Hall, B. D., & Dutton, G.: 3-D atmospheric modeling of the global budget of N_2O and its isotopologues for 1980–2019: The impact of anthropogenic emissions. Global Biogeochemical Cycles, 36, e2021GB007202. https://doi.org/10.1029/2021GB007202, 2022.

Lickley, M., Solomon, S., Kinnison, D., Krummel, P., Mühle, J., O'Doherty, S., et al.: Quantifying the imprints of stratospheric contributions to interhemispheric differences in tropospheric CFC-11, CFC-12, and N_2O abundances. Geophysical Research Letters, 48, e2021GL093700. https://doi. org/10.1029/2021GL093700, 2021.

Lovenduski, N.S., Gruber, N., Doney, S.C., and Lima, I.D.: Enhanced CO_2 outgassing in the Southern Ocean from a positive phase of the Southern Annular Mode, Glob. Biogeochem. Cycles 21, GB2026, doi:10.1029/2006GB002900, 2007.

Lueker, T.J., Walker, S.J., Vollmer, M.K., Keeling, R.F., Nevison, C.D. and Weiss, R.F.: Coastal upwelling air-sea fluxes revealed in atmospheric observations of O_2/N_2, CO_2 and N_2O, Geophys. Res. Lett., 30, 1292, 2003.

https://doi.org/10.5194/egusphere-2023-2877
Preprint. Discussion started: 8 December 2023

MacFarling Meure, C., Etheridge, D. M., Trudinger, C. M., Steele, L. P., Langenfelds, R. L., van Ommen, T., Smith, A. and Elkins, J. W.: Law Dome CO_2, CH_4, and N_2O ice core records extended to 2000 years BP, Geophys. Res. Lett., 33, L14810, doi:10.1029/2006GL026152, 2006.

Mahowald, N. M., Rasch, P. J., Eaton, B. E., Whittlestone, S. and Prinn, R. G.: Transport of radon-222 to the remote troposphere using the Model of Atmospheric Transport and Chemistry and assimilated winds from ECMWF and the National Center for Environmental Prediction/NCAR, J. Geophys. Res., 102, 28139–28151, 1997.

Masarie, K. A. and Tans, P.P.: Extension and integration of atmospheric carbon dioxide data into a globally consistent measurement record, Journal of Geophysical Research-Atmospheres, 100, D6, 11593-11610, 1995.

McPhaden, M. J., et al.: The tropical ocean-global atmosphere observing system: A decade of progress, J. Geophys. Res., 103, 14,169–14,240, doi:10.1029/97JC02906, 1998.

Mosier, A.R., Duxbury, J.M., Freney, J.R., Heinemeyer, O. and Minami, K.: Assessing and mitigating N_2O emissions from agricultural soils, Climatic Change, 40, 7-38, 2000.

Naqvi, S.W.A., Jayakumar, D.A., Narvekar, P.V., Naik, H., Sarma, V.V.S.S., D'Sousa, W., Joseph, S., and George, M.D.: Increased marine production of N_2O due to intensifying anoxia on the Indian continental shelf, Nature, 408, 346-349, 2000.

Nash, E.R., Newman, P.A., Rosenfield, J.E., and Schoeberl, M.R.: An objective determination of the polar vortex using Ertel's potential vorticity, J. Geophys. Res., 101, 9471-9478, 1996.

National Oceanic Atmospheric Administration (NOAA) Global Monitoring Division, Interactive Data Visualization, https://www.esrl.noaa.gov/gmd/dv/iadv/, accessed April 6, 2021.

Nevison, C.D., Weiss, R.F. and Erickson III, D.J.: Global Oceanic Nitrous Oxide Emissions, J. Geophys. Res., 100, 15,809-15,820, 1995.

Nevison, C.D., Kinnison, D.E. and Weiss, R.F.: Stratospheric Influence on the tropospheric seasonal cycles of nitrous oxide and chlorofluorocarbons, Geophys. Res. Lett. 31(20), L20103, doi:10.1029/2004GL020398, 2004.

Nevison, C.D., Keeling, R.F., Weiss, R.F., Popp, B.N., Jin, X., Fraser, P.J, Porter, L.W. and Hess, P.G.: Southern Ocean ventilation inferred from seasonal cycles of atmospheric N_2O and O_2/N_2 at Cape Grim, Tasmania, Tellus, 57B, 218-229, 2005.

Nevison, C. D., Mahowald, N. M., Weiss, R.F. and Prinn, R.G.: Interannual and seasonal variability in atmospheric N_2O, Global Biogeochem. Cy., 21, GB3017, doi:10.1029/2006GB002755, 2007.

Nevison, C.D., Dlugokencky, E., Dutton, G., Elkins, J.W., Fraser, P., Hall, B., Krummel, P.B., Langenfelds, R.L., O'Doherty, S., Prinn, R.G., Steele, L.P., Weiss, R.F.: Exploring causes of interannual variability in the seasonal cycles of tropospheric nitrous oxide, Atmospheric Chemistry and Physics, 11, doi:10.5194/acp-11-1-2011, 1-18, 2011.

Nevison, C., Andrews, A., Thoning, K., Dlugokencky, E., Sweeney, C., Miller, S., et al.: Nitrous oxide emissions estimated with the CarbonTracker-Lagrange North American regional inversion framework. Global Biogeochemical Cycles, 32. https://doi. org/10.1002/2017GB005759, 2018.

Newman, P.: The Quasi-biennial Oscillation (QBO). Retrieved from https://acd-ext.gsfc.nasa.gov/Data_services/met/qbo/qbo.html, 2020.

https://doi.org/10.5194/egusphere-2023-2877
Preprint. Discussion started: 8 December 2023

Nielsen, J.E., Pawson, S., Molod, A., Auer, B., da Silva, A.M., Douglass, A.R., et al.: Chemical mechanisms and their applications in the Goddard Earth Observing System (GEOS) Earth system model, Journal of Advances in Modeling Earth Systems, 9(8), 3019-3044, doi:10.1002/2017MS001011, 2017.

Olivier, J.G.J., Van Aardenne, J.A., Dentener, F., Ganzeveld, L. and Peters, W.: Recent trends in global greenhouse gas emissions: regional trends and spatial distribution of key sources. In: Non-CO_2 Greenhouse Gases (NCGG-4), van Amstel, A. (coord.), page 325-330. Millpress, Rotterdam, 2005.

Park, S., et al.: Trends and seasonal cycles in the isotopic composition of nitrous oxide since 1940, Nature Geoscience, 5, 261-265, 2012.

Plumb, R. A.: Stratospheric transport, J. Meteorol. Soc. Jpn., 80, 793–809, 2002.

Prather, M. Hsu, J., J., DeLuca, N.M., Jackman, C.H., Oman, L.D., Douglass, A.R., Fleming, E.L., Strahan, S.E., Steenrod, S.D., Sovde, O.A., Isaksen, I.S.A., Froidevaux, L., Funke, B.: Measuring and modeling the lifetime of nitrous oxide including its variability, J. Geophys. Res. Atmos., 120, doi:10.1002/2015JD023267, 2015.

Prinn, R.G., Weiss, R.F., Fraser, P.J., Simmonds, P.G., Cunnold, D.M., Alyea, F.N., O'Doherty, S., Salameh, P., Miller, B.R., Huang, J., Wang, R.H.J., Hartley, D.E., Harth, C., Steele, L.P., Sturrock, G., Midgley, P.M. and McCulloch, A.: A history of chemically and radiatively important gases in air deduced from ALE/GAGE/AGAGE, J. Geophy. Res., 105 (D14), 17751-17792, 2000.

Ravishankara A. R., Daniel, J. S. and Portmann, R. W.: Nitrous Oxide (N_2O): The dominant ozone depleting substance emitted in the 21st century, Science, 326,123-125, doi: 10.1126/science.1176985, 2009.

Ray, E. A., Portmann, R. W., Yu, P., Daniel, J., Montzka, S. A., Dutton, G. S., et al.: The influence of the stratospheric Quasi-Biennial Oscillation on trace gas levels at the Earth's surface. Nature Geoscience, 13(1), 22–27. https://doi.org/10.1038/s41561-019-0507-3, 2020.

Ruiz, D.J., Prather, M.J., Strahan, S.E., Thompson, R.L., Froidevaux, L., and Steenrod, S.D.: How atmospheric chemistry and transport drive surface variability of N_2O and CFC-11, J. Geophys. Res., 2021.

Santoni, G. W., Daube, B. C., Kort, E. A., Jiménez, R., Park, S., Pittman, J. V., Gottlieb, E., Xiang, B., Zahniser, M. S., Nelson, D. D., McManus, J. B., Peischl, J., Ryerson, T. B., Holloway, J. S., Andrews, A. E., Sweeney, C., Hall, B., Hintsa, E. J., Moore, F. L., Elkins, J. W., Hurst, D. F., Stephens, B. B., Bent, J., and Wofsy, S. C.: Evaluation of the airborne quantum cascade laser spectrometer (QCLS) measurements of the carbon and greenhouse gas suite – CO_2, CH_4, N_2O, and CO – during the CalNex and HIPPO campaigns, Atmos. Meas. Tech., 7, 1509–1526, https://doi.org/10.5194/amt-7-1509-2014, 2014.

Sokal, R.R. and Rohlf, F.J.: Biometry, 859 pp., W.H. Freeman, New York, 1981.

Stephens, B.: ORCAS Merge Products. Version 1.0, https://doi.org/10.5065/D6SB445X, accessed 13 Jul 2020, 2017.

Stephens, B. B., Long, M. C., Keeling, R. F., Kort, E. A., Sweeney, C., Apel, E. C., Atlas, E. L., Beaton, S., Bent, J. D., Blake, N. J., Bresch, J. F., Casey, J., Daube, B. C., Diao, M., Diaz, E., Dierssen, H., Donets, V., Gao, B.-C., Gierach, M., Green, R., Haag, J., Hayman, M., Hills, A. J., Hoecker-Martínez, M. S., Honomichl, S. B., Hornbrook, R. S., Jensen, J. B., Li, R.-R., McCubbin, I., McKain, K., Morgan, E. J., Nolte, S., Powers, J. G., Rainwater, B., Randolph, K., Reeves, M.,

https://doi.org/10.5194/egusphere-2023-2877
Preprint. Discussion started: 8 December 2023

Schauffler, S. M., Smith, K., Smith, M., Stith, J., Stossmeister, G., Toohey, D. W., and Watt, A. S.: The O2/N2 Ratio and CO2 Airborne Southern Ocean Study, B. Am. Meteorol. Soc., 99, 381–402, https://doi.org/10.1175/BAMS-D-16-0206.1, 2018.

Stohl, A.: A 1-year Lagrangian "climatology" of airstreams in the Northern Hemisphere tropo- sphere and lowermost stratosphere, J. Geophys. Res., 106(D7), 7263–7279, 2001.

Strahan, S. E., Oman, L.D., Douglass, A.R. and Coy, L.: Modulation of Antarctic vortex composition by the quasi-biennial oscillation, Geophys. Res. Lett., 42, 4216–4223, doi:10.1002/2015GL063759, 2015.

Thompson, R.L., Dlugokencky, E., Chevallier, F., Ciais, P., Dutton, G., Langenfelds, R.L., Prinn, R.G., Weiss, R.F., Tohjima, Y., O'Doherty, S., Krummel, P.B., Fraser, P., and Steele, L.P.: Interannual variability in tropospheric nitrous oxide, 2013, Geophys. Res. Lett., 40, 4426-4431, doi:10.1002/grl.50721, 2013.

Thompson, R. L., Patra, P. K., Ishijima, K., Saikawa, E., Corazza, M., Karstens, U., et al.: TransCom N2O model inter-comparison-Part 1: Assessing the influence of transport and surface fluxes on tropospheric N2O variability, Atmospheric Chemistry and Physics, 14(8), 4349–4368. https://doi.org/10.5194/acp-14-4349-2014.

Thompson, R.L., Lassaletta, L., Patra, P.K., Wilson, C., Wells, K.C., Gressent, A., Koffi, E.N., Chipperfield, M.P., Winiwarter, W., Davidson, E.A., Tian, H. and Canadell, J.G.: Acceleration of global N_2O emissions seen from two decades of atmospheric inversion, Nature Climate Change, https://doi.org/10.1038/s41558-019-0613-7, 2019.

Thompson, T.M., Elkins, J.W., Hall, B., Dutton, G.S., Swanson, T.H., Butler, J.H., Cummings, S.O., Fisher, D.A.: Halocarbons and other Atmospheric Trace Species, in: Schnell, R.C., A.-M. Buggle and R.M. Rossson (Eds.), Climate Diagnostics Laboratory Summary Report #27, 2002-2003, US Department of Commerce, National Oceanic and Atmospheric Administration, Boulder, Colorado, 2004.

Thompson, C.R., Wofsy, S.C., Prather, M.J., Newman, P.A., Hanisco, T.F., Ryerson, T.B., Fahey, D.W., Apel, E.C., Brock, C.A., Brune, W.H. et al.: The NASA Atmospheric Tomography (ATom) mission: Imaging the chemistry of the global atmosphere, Bulletin of the American Meteorological Society, 103 (3): E761–E790. DOI: http://dx.doi.org/10.1175/bams-d-20-0315.1, 2022.

Tian, H., Xu, R., Canadell, J.G., Thompson, R.L., Winiwarter, W., Suntharalingam, P., Davidson, E.A., Ciais, P., et al.: A comprehensive quantification of global nitrous oxide sources and sinks, Nature, 586, 248-255. https://doi.org/10.1038/s41586-020-2780-0, 2020.

Volk, C.M., Elkins, J.W., Fahey, D., Dutton, G., Gilligan, J., Lowenstein, M., Podolske, J., Chan, K., and Gunson, M.: Evaluation of source gas lifetimes from stratospheric observations, J. Geophys. Res., 102(D21), 25,543-25,564, 1997.

Waugh, D.W., Randel, W.J., Pawson, S., Newman, P.A. and Nash, E.R.: Persistence of the lower stratospheric polar vortices, J. Geophys. Res., 104 (D22), 27,191-27,201, 1999.

Weiss, R.F.: The temporal and spatial distribution of tropospheric nitrous oxide, J. Geophys. Res. 86, 7185-7195, 1981.

Wofsy, S. C., the HIPPO Science Team and Cooperating Modellers and Satellite Teams: HIAPER Pole-to-Pole Observations (HIPPO): Fine grained, global scale measurements for determining rates for transport, surface emissions, and removal of

https://doi.org/10.5194/egusphere-2023-2877
Preprint. Discussion started: 8 December 2023

climatically important atmospheric gases and aerosols, Phil. Trans. of the Royal Society A, 369(1943), doi:10.1098/rsta.2010.0313, 2073-2086, 2011.

Wofsy, S., Afshar, S., Allen, H., Apel, E., Asher, E., Barletta, B., Bent, J., Bian, H., Biggs, B., Blake, D., and et al.: ATom: Merged Atmospheric Chemistry, Trace Gases, and Aerosols, https://doi.org/10.3334/ORNLDAAC/1581, accessed 13 Jul 2020, 2018.

Wofsy, S., Daube, B., Jimenez, R., Kort, E., Pittman, J., Park, S., Commane, R., Xiang, B., Santoni, G., Jacob, D., and et al.: HIPPO Merged 10-Second Meteorology, Atmospheric Chemistry, and Aerosol Data. Version 1.0, https://doi.org/10.3334/CDIAC/HIPPO_010, accessed 13 Jul 2020, 2017.

WMO Greenhouse Gas Bulletin No. 14, https://library.wmo.int/ doc_num.php?explnum_id=5455, 2018.

Yang, S. et al.: Global reconstruction reduces the uncertainty of oceanic nitrous oxide emissions and reveals a vigorous seasonal cycle, Proceedings of the National Academy of Sciences, 117(22), 11954–11960, doi:10.1073/pnas.1921914117, 2020.